



THE HEBREW UNIVERSITY OF JERUSALEM,
FACULTY OF SCIENCE

THE RACAH INSTITUTE OF PHYSICS

**An Algebraic Approach to
First-Order Quantum Phase
Transitions Between Two
Deformed Nuclear Shapes**

**ג'ישה אלגברית למעבר פאזה קוונטי
מסדר-ראשון בין שתי צורות
גרעיניות מעוותות**

Thesis submitted in partial fulfillment of the requirements
for the degree of M.Sc

Author:
Dekel Shapira
ID: 036552628

Supervisor:
Professor Amiram
Leviatan

January, 2015

שבט, תשע"ה

Acknowledgment

I would like to thank my supervisor, Professor Amiram Leviatan, for the many hours he spent teaching me, for his enthusiasm which taught me more than just physics, and for his endless patience that helped guiding me throughout this work. I would also like to thank my colleague and roommate, Noam Gavriellov, for many long discussions. I am grateful to Professor José Enrique García Ramos for the use of his computer program.

תקציר

עם התקדמות שיטות המחקר הנסיוניות בשנים האחרונות, התגלו בגרעינים כבדים רבים קיום, זה לצד זה, של שתי צורות ציריות-מעוותות. בעזרת מודל הבוזונים של הגרעין (IBM) ניתן לתאר גרעינים בינוניים-כבדים עם מספר זוגי של פרוטונים וניוטרונים. מודל זה שימש באופן נרחב כדי לתאר את האנרגיות והמעברים האלקטרו-מגנטים בגרעינים כאלה. עד כה השימוש העיקרי ב-IBM נעשה באמצעות המילטוניאן המכיל אינטרקציות דו-גופיות בין הבוזונים. בהקשר של מעבר פאזה בין שתי צורות שונות בגרעין, המילטוניאן כזה יכול לתאר דו-קיום של צורה כדורית ומעוותת בלבד. כדי לתאר מעבר פאזה מסדר-ראשון בין שתי צורות גרעיניות מעוותות יש צורך בשימוש בהמילטוניאן תלת-גופי. בהמילטוניאן התלת-גופי של ה-IBM קיימות 17 אינטראקציות שונות בלתי-תלויות. כדי למצוא את האינטרקציות האחראיות למעבר פאזה בין צורות מעוותות אם כן, יש לנקוט בגישה מושכלת. בעבודה זו נמצא את האינטראקציות שבעזרתן ניתן לתאר את הנקודה הקריטית במעבר פאזה מסדר-ראשון בין שתי צורות מעוותות. נעשה זאת באמצעות חלוקת ההמילטוניאן הקריטי להמילטוניאן אינטרינסי וקולקטיבי, ובאמצעות שימוש במצבים קוהרנטים. ננתח את ההמילטוניאן האינטרינסי באמצעות שיטות שונות, ולאחר מכן נבחן את השינויים הנגרמים בעקבות הוספת האיברים הקולקטיביים.

Abstract

With the advancement of experimental techniques over the last few years, many medium-heavy nuclei in and outside the region of stability were found to have a coexistence of axially-deformed shapes.

The interacting boson model (IBM) has been used extensively for describing medium-heavy even-even nuclei. The vast majority of applications have employed an Hamiltonian with two-body interactions. In conjunction with quantum phase transitions, such an Hamiltonian can accommodate coexistence of one spherical and one axially-deformed shapes.

The two-body IBM Hamiltonian, however, cannot describe first-order shape phase transitions between prolate and oblate shapes. To achieve these, a three-body Hamiltonian is needed. The three-body IBM has 17 independent terms, which requires selection criteria in order to find the relevant operators.

In this work we address this problem by a novel method based on the resolution of the Hamiltonian into intrinsic and collective parts and coherent states. The intrinsic Hamiltonian is first analyzed by various approaches, and the affect of adding the collective parts is then examined.

Contents

Background and Motivation	1
1 Interacting Boson Model	3
1.1 Algebraic Structure	3
1.2 Geometric Interpretation	6
1.2.1 The IBM Intrinsic State and Energy Surface	6
1.2.2 General Non-Spherical Basis	7
1.3 Intrinsic and Collective Resolution of the Hamiltonian	9
1.4 Electromagnetic Transitions	10
1.5 Partial Dynamical Symmetries	12
2 Quantum Shape Phase Transitions	14
2.1 2-Body IBM Hamiltonian	15
2.2 3-Body IBM Hamiltonian	16
3 Constructing the Critical Hamiltonian	17
4 Energy Surface of the Critical Hamiltonian	22
4.1 Energy Surface of $R_0^\dagger R_0$	23
4.2 Energy Surface of $R_2^\dagger \cdot \tilde{R}_2$	25
4.3 Energy Surface of the Critical Hamiltonian	29
4.4 Normal Modes Expansion of the Intrinsic Hamiltonian	32
4.4.1 Normal Modes of $R_0^\dagger R_0$	32

<i>CONTENTS</i>	v
4.4.2 Normal Modes of $R_2^\dagger \cdot R_2$	33
4.4.3 Normal Modes Expansion of the Intrinsic Hamiltonian	34
5 Analysis of the Intrinsic Hamiltonian	36
5.1 Identification of the Bands	40
6 Collective Terms for the Critical Hamiltonian	46
6.1 Two-State Mixing	51
7 Conclusions and Outlook	56
Bibliography	60
Appendix A Critical Hamiltonian Energy Surface	64
Appendix B $O(6)$-$\langle\sigma\rangle$ Decomposition of the Intrinsic States	70
Appendix C Matrix Elements of the Collective Hamiltonian	73

Background and Motivation

Quantum phase transitions (QPT) are widely researched in various areas of Physics. For example condensed matter physics [1], quantum optics [2] and nuclear physics [3]. They are characterized by a structural change of the system at zero temperature, which occurs when a coupling constant in the Hamiltonian is varied.

In nuclei, the effective Hamiltonian is a function of the proton and neutron numbers, and the coupling constant is a function of these numbers. Experimentally, nuclear phase transitions are indicated by the spectrum, e.m. transitions, two-neutron separation energies and the isotope and isomer shifts. The different phases correspond to “shapes” of the nucleus, and the possible quadruple shapes are prolate, oblate, spherical and triaxial. Phase transitions in nuclei were first observed for nuclei with 90 neutrons and about 60 protons [3]. In first-order phase transitions in nuclei, the critical point is characterized by a coexistence of the nuclear shapes.

In recent years, with the advancement of experimental methods, an abundance of experimental data that shows an evidence of shape coexistence between two deformed-shapes was collected. For example, the light Krypton isotopes [4, 5], or the triple coexistence found in ^{186}Pb [6] or ^{43}S [7].

There are many approaches to the study of heavy nuclei, for example the *nuclear density functional theory*, *geometric model* and the *interacting boson model*. The interacting boson model (IBM) [8] is an algebraic approach, it describes even-even nuclei and can be solved exactly by diagonalization of relatively small matrices.

The two-body IBM Hamiltonian is the simplest and most used Hamiltonian in this model. It consists of seven parameters in the Hamiltonian, and was used extensively to describe first and second order phase transitions in nuclei (see for example [9, 10]). The two-body IBM, however, cannot be used to model the experimental data of two coexisting deformed phases, and as a result cannot be used for first order phase transitions between two deformed shapes (henceforth deformed-deformed). For this, three-body IBM is needed [11].

The three-body Hamiltonian is much more complex than the two-body. It contains a total of 17 independent terms. To use this Hamiltonian with the experimental data, it is important to choose the correct parameters.

This work explores the possibilities for a first-order phase transition in nuclei using the IBM. In particular, we present a novel method to construct a three-body IBM Hamiltonian that accommodates coexistence of two deformed shapes, and analyze the resulting Hamiltonian.

Chapter 1

Interacting Boson Model

The *interacting boson model* (IBM) is a nuclear model proposed by Arima and Iachello in 1974 [8]. It uses an algebraic and group theoretical approach to model even-even nuclei. This approach is realized by using a number-conserving Hamiltonian with an $SO(3)$ symmetry, and bosonic creation and annihilation operators.

The IBM assumes that the low-lying ‘collective’ states in even-even nuclei can be described by bosons of angular momentum 0 and 2. This assumption gains support from the features of generalized seniority calculations in the shell-model, and of the spectra of near-closed shell nuclei, in which the 0^+ and 2^+ states lie much lower than higher angular momentum states [12]. Each boson in the model represents a pair of valence nucleons, and the valence nucleons are counted from the nearest closed shell. The counting is done for protons and neutrons separately; for example $^{128}_{54}\text{Xe}$ has 4 valence protons ($54 - 50$), and 8 (hole) valence neutrons ($82 - 74$). Hence, to model this nucleus in the IBM, the number of bosons is 6 ($N = \frac{8+4}{2}$).

1.1 Algebraic Structure

As mentioned above, the IBM describes a system of N bosons, where N is determined separately for each nucleus. The model is best described

in second quantization. It consists of six bosonic creation-operators s^\dagger, d_μ^\dagger ($\mu = -2, \dots, 2$) with an angular momentum $L = 0, 2$, along with six destruction operators s, d_μ . The state $|0\rangle$ represents a closed-shell. The usual commutation relations $[d_\mu, s^\dagger] = 0$, $[d_\mu, d_{\mu'}^\dagger] = \delta_{\mu\mu'}$, $[s, s^\dagger] = 1$ are imposed and $s|0\rangle = d_\mu|0\rangle = 0$.

The Hamiltonian is built from n -body interactions, and is $SO(3)$ scalar and N -conserving. In their original formulation, Arima and Iachello considered one and two-body interactions [8], as it is the simplest Hamiltonian which offers nontrivial results. It is noted that the destruction operator d does not transform according to the $L = 2$ irreducible representation (irrep) of $SO(3)$. To amend this it is customary to use instead the tilde operators $\tilde{d}_\mu = (-1)^\mu d_{-\mu}$. These set of operators does transform as the $L = 2$ tensor, and as such can be manipulated using Clebsch-Gordan coupling.

The most general two-body IBM Hamiltonian can be written as

$$\begin{aligned}
H = & \epsilon_s s^\dagger s + \epsilon_d d^\dagger \cdot \tilde{d} + u_0 (s^\dagger)^2 s^2 + u_2 (s^\dagger d^\dagger) \cdot s \tilde{d} + v_0 [d^\dagger \cdot d^\dagger s^2 + (s^\dagger)^2 \tilde{d} \cdot \tilde{d}] \\
& + v_2 [(d^\dagger d^\dagger)^{(2)} \cdot \tilde{d} s + s^\dagger d^\dagger \cdot (\tilde{d} \tilde{d})^{(2)}] + \sum_{L=0,2,4} c_L (d^\dagger d^\dagger)^{(L)} \cdot (\tilde{d} \tilde{d})^{(L)}
\end{aligned} \tag{1.1}$$

where $\epsilon_s, \epsilon_d, u_0, u_2, v_0, v_2, c_L$ ($i = 0, 2, 4$) are parameters. The notion $(AB)^{(L)}$ is used to couple the two tensor-operators A and B to a new tensor-operator with an angular momentum L . That is

$$(A^{(l_1)} B^{(l_2)})_M^{(L)} \equiv \sum_{m_1, m_2} (l_1 m_1 l_2 m_2 | LM) A_{m_1}^{(l_1)} B_{m_2}^{(l_2)}$$

where $(l_1 m_1 l_2 m_2 | LM)$ are Clebsch-Gordan coefficients. The dot-product is defined as $A^{(L)} \cdot B^{(L)} = (-1)^L \sqrt{2L+1} (A^{(L)} B^{(L)})^{(0)}$, and the dependence on the number of bosons comes into play in the Hilbert space in which H acts. The 36 operators $s^\dagger s, d_\mu^\dagger d_\nu, s^\dagger d_\mu, d_\mu^\dagger s$ fulfill the commutation relations of the $SU(6)$ generators, as a consequence, the set of basis states with given N transform as the row of the symmetric irrep of $U(6)$. This irrep can be labeled by N . In addition, since the Hamiltonian is an $SO(3)$ scalar, each

of the eigenstates can be classified by an $SO(3)$ label. It is of advantage to find all the subgroups of $U(6)$ that include $SO(3)$ as a subgroup. This allows us to label a basis of states (and operators) by a ‘chain’ of groups. That is, label each state with a set of quantum numbers where each of the numbers corresponds to a group’s irrep. The three chains in the IBM and their labels are [13]:

$$\begin{aligned}
 U(6) &\supset U(5) \supset O(5) \supset O(3) \\
 [N] &\quad \langle n_d \rangle \quad (\tau) \quad n_\Delta \quad L \\
 U(6) &\supset SU(3) \supset O(3) \\
 [N] &\quad (\lambda, \mu) \quad K \quad L \\
 U(6) &\supset O(6) \supset O(5) \supset O(3) \\
 [N] &\quad \langle \sigma \rangle \quad (\tau) \quad n_\Delta \quad L
 \end{aligned} \tag{1.2}$$

Here, the irrep labels appear below the group names. For a given chain, a complete orthogonal basis can be found such that each state is labeled by the irreps of that chain. The process of deducing the possible labels for each chain is called “reduction to irreducible representations”, and the label of a group irrep determines the possible labels of its subgroups.

The labels n_Δ and K are special as they do not correspond to any group (*missing labels*). However, they are sometimes necessary to distinguish between states, the labels of which are otherwise the same (ultimately this depends on the dimension of the Hilbert space). A convenient choice for K in the IBM is the Elliott basis [14]. Within this choice K is the same as the angular momentum projection on the symmetry axis. States with different K , but otherwise same group labels, are not necessarily orthogonal (after $SO(3)$ rotation).

When the Hamiltonian is composed of the Casimir operators that corresponds to one specific chain, then the eigenstates can be labeled by the irreps of that chain. Such Hamiltonians are solvable in the sense that the energies and transitions between states are known analytically. Changing the coefficients of the Casimir operators change only the eigenvalues. These types of situations are called *dynamical symmetries*

1.2 Geometric Interpretation

1.2.1 The IBM Intrinsic State and Energy Surface

The IBM is an algebraic collective model, as opposed to the geometric collective model [15], it does not contain any reference to geometry. A useful concept that helps bridge the gap between the IBM and the geometric model, and gives the IBM states geometrical meaning is the *intrinsic state*. The (normalized) intrinsic state is a condensate defined by [16]:

$$\begin{aligned}
 |\beta, \gamma; N\rangle &= \frac{(b_c^\dagger)^N}{\sqrt{N!}} |0\rangle \\
 b_c^\dagger &= \frac{1}{\sqrt{1 + \beta^2}} [s^\dagger + \beta \cos \gamma d_0^\dagger + \frac{\beta}{\sqrt{2}} \sin \gamma (d_2^\dagger + d_{-2}^\dagger)] \\
 \beta &\in [0, \infty), \quad \gamma \in [0, \pi/3]
 \end{aligned} \tag{1.3}$$

This state is intrinsic in the sense that it depends on the *quadruple shape variables* β and γ , and that any of the IBM states can be projected from it by properly averaging β, γ and the Euler angles. The limitation on the β and γ parameters prevents the intrinsic state from having the same “shape” in different orientations. For example, it can be seen that the intrinsic state $|\beta, \pi/3; N\rangle$ is the same as $|\beta, 0; N\rangle$ after $\pi/2$ rotation by the three Euler angles: $\hat{R}(\psi = \pi/2, \phi = \pi/2, \theta = \pi/2)$.

The intrinsic state can be used as a trial function for a variational method. The expectation value of the IBM Hamiltonian defines a two-parameter energy surface

$$E^N(\beta, \gamma) = \langle \beta, \gamma; N | H | \beta, \gamma; N \rangle \tag{1.4}$$

The global minimum of this expression $E^N(\beta_0, \gamma_0)$, gives an upper bound on the ground state energy. For $N \rightarrow \infty$, the minimum of the energy surface converges to the exact ground state energy.

The *equilibrium shape* of the Hamiltonian is defined by the parameters β_0

and γ_0 that minimize the energy surface. Any intrinsic state $|\beta_0, \gamma_0; N\rangle$ can be associated with a shape, determined by its β_0 and γ_0 parameters. The possible shapes for the two-body IBM are *spherical* shape for $\beta_0 = 0$, and an axially deformed shape for $\beta_0 > 0$, which can be either prolate shape ($\gamma_0 = 0$) or oblate shape ($\gamma_0 = \pi/3$).

For the two-body Hamiltonians that correspond with the dynamical symmetries, the equilibrium shapes (for large- N) are [16]:

$$\begin{aligned} U(5) : \beta_0 &= 0 \\ O(6) : \beta_0 &= 1, \gamma_0 = \text{arbitrary} \\ SU(3) : \beta_0 &= \sqrt{2}, \gamma_0 = 0 \end{aligned} \quad (1.5)$$

The $U(5)$ limit can be associated with a spherical shape, as noted above. This limit is called the *an-harmonic spherical vibrator* [17]. The $SU(3)$ limit can be identified with the *axially-deformed rotovibrator* [18] and the $O(6)$ limit can be identified with γ -*unstable deformed rotovibrator* [19].

It is noted that the state $|\beta = 1, \gamma = 0; N\rangle$ is the lowest weight state in the $SO(6)$ irrep $\langle \sigma = N \rangle$, and the state $|\beta = \sqrt{2}, \gamma = 0; N\rangle$ is the lowest weight state in the $SU(3)$ irrep $(\lambda = 2N, \mu = 0)$ (see [20] and [21]). In addition the energy surface is invariant to rotations, and as a consequence it will have the same value if the intrinsic states are rotated. For example $E(-\beta, 0) = E(\beta, \pi/3)$.

1.2.2 General Non-Spherical Basis

The general non-spherical basis (GNSB) is defined to be [22]:

$$\begin{aligned} b_c^\dagger &= \frac{\beta \cos \gamma d_0^\dagger + \beta \sin \gamma (d_2^\dagger + d_{-2}^\dagger)/\sqrt{2} + s}{(1 + \beta^2)^{1/2}} & b_x^\dagger &= \frac{1}{\sqrt{2}}(d_1^\dagger + d_{-1}) \\ b_\beta^\dagger &= \frac{\cos \gamma d_0^\dagger + \sin \gamma (d_2^\dagger + d_{-2}^\dagger)/\sqrt{2} - \beta s}{(1 + \beta^2)^{1/2}} & b_y^\dagger &= \frac{1}{\sqrt{2}}(d_1^\dagger - d_{-1}) \\ b_\gamma^\dagger &= \frac{1}{\sqrt{2}} \cos \gamma (d_2^\dagger + d_{-2}^\dagger) - \sin \gamma d_0^\dagger & b_z^\dagger &= \frac{1}{\sqrt{2}}(d_2^\dagger - d_{-2}) \end{aligned} \quad (1.6)$$

It is a complete and orthonormal basis ($[b_i, b_j^\dagger] = \delta_{ij}$) that depends on the two shape variables β, γ . As such, for any choice of β and γ , the IBM Hamiltonian can be expressed in these operators. We note that the members of the non-spherical basis do not have a well defined angular momentum (for $\beta > 0$).

It is possible to approximate the lowest eigenstates and energies of any Hamiltonian by using the Bogoliubov approximation. This is done by first looking for the equilibrium values (β_0, γ_0) of the Hamiltonian, then re-writing it in terms of the twelve GNSB operators $b_i, b_i^\dagger(\beta_0, \gamma_0)$. The next step consists of replacing the condensate operators b_c^\dagger and b_c with \sqrt{N} , and then retaining the highest order of N . This approximation is similar to the normal-mode expansion around the minimum of the potential energy.

The condensate $|\beta_0, \gamma_0; N\rangle$ can be decomposed into states with definite L . These set of states are identified with the ground-band of the Hamiltonian in a variational sense.

When $\beta_0 > 0$ and $\gamma_0 = \{0, \pi/3\}$, it is also possible to define the β - and γ -intrinsic states that are associated with the equilibrium shape. These states are defined by applying the b_β^\dagger or b_γ^\dagger operators to the intrinsic ground-state with $N - 1$ bosons:

$$\begin{aligned} |b_\beta; N\rangle &= b_\beta^\dagger b_c |\beta_0, \gamma_0; N\rangle \\ |b_\gamma; N\rangle &= b_\gamma^\dagger b_c |\beta_0, \gamma_0; N\rangle \end{aligned} \tag{1.7}$$

The resulting states can be used to define the β - and γ - bands of the equilibrium values by an $SO(3)$ projection. For these cases, the ground- and β - bands have the $K = 0$ label, and as such are composed of the angular-momentum states with $L = 0, 2, 4, \dots$. The γ -band, in this case, has $K = 2$ and is composed of the states with $L = 2, 3, 4, \dots$ [11]. The angular-momenta of the ground-, β - and γ -bands described above are in accordance with those of the geometrical model (except for a finite- N effect).

1.3 Intrinsic and Collective Resolution of the Hamiltonian

Using the notion of intrinsic states and energy surface, it is possible to split the IBM Hamiltonian into intrinsic and collective parts: $H = H_{int} + H_{col}$ [23]. By definition, the intrinsic part has the same energy surface, up to a constant, as the full Hamiltonian, and has the equilibrium states as eigenstates with zero energy: $H_{int}|\beta_0, \gamma_0; N\rangle = 0$. It affects the classical “potential energy”, $V(\beta, \gamma)$. The collective part is the rest of the Hamiltonian, and its energy surface is independent of β and γ (that is, a constant).

The resolution into intrinsic and collective parts can be used to build different Hamiltonians: the intrinsic part of the Hamiltonian serves to create well defined bands, while the collective part serves to split and mix the bands. This is an important feature as many even-even nuclei tend to have well defined band structure.

To build an intrinsic Hamiltonian, we require the Hamiltonian to satisfy

$$H_{int}|\beta_0, \gamma_0; N\rangle = 0 \quad (1.8)$$

One way to do it is to find *annihilation operators* [22], T_i , such that

$$T_i|\beta_0, \gamma_0; N\rangle = 0 \quad (1.9)$$

The operators can then be combined to form a scalar number-conserving Hamiltonian, $H_{int} = \sum_{ij} C_{ij} T_j^\dagger T_i$, where the coefficients C_{ij} are chosen so that H is an $SO(3)$ scalar.

For the two-body IBM, there are two annihilation operators with definite angular momentum, $L = 0, 2$. The operators and their matching energy

surface are [22]:

$$\begin{aligned}
 P_0(\beta_0) &= \tilde{d} \cdot \tilde{d} - \beta_0^2 s^2 \\
 E_0(\beta, \gamma) &= \langle \beta, \gamma | P_0^\dagger P_0 | \beta, \gamma \rangle = N(N-1) \frac{\beta^4 - 2\beta_0^2 \beta^2 + \beta_0^4}{(1 + \beta^2)^2}
 \end{aligned} \tag{1.10}$$

$$\begin{aligned}
 \tilde{P}_{2\mu}(\beta_0) &= \beta_0 \sqrt{2} s \tilde{d}_\mu + \sqrt{7} (\tilde{d} \tilde{d})_\mu^{(2)} \\
 E_2(\beta, \gamma) &= \langle \beta, \gamma | P_2^\dagger \cdot \tilde{P}_2 | \beta, \gamma \rangle = N(N-1) 2\beta^2 \frac{\beta^2 - 2\beta_0 \beta \cos 3\gamma + \beta_0^2}{(1 + \beta^2)^2}
 \end{aligned} \tag{1.11}$$

From this expression it can be seen that $P_0(\beta_0)$ annihilates the condensates $|\beta_0, \gamma; N\rangle$ (for any γ), and $\tilde{P}_2(\beta_0)$ annihilates the condensates $|0; \gamma; N\rangle$ and $|\beta_0, 0; N\rangle$ (if $\beta_0 > 0$) or $|\beta_0, \pi/3; N\rangle$ (if $\beta_0 < 0$).

The intrinsic two-body Hamiltonian is given by the combination of the two operators

$$H_{int} = h_0 P_0^\dagger(\beta_0) P_0(\beta_0) + h_2 P_2^\dagger(\beta_0) \cdot \tilde{P}_2(\beta_0) \tag{1.12}$$

1.4 Electromagnetic Transitions

The electromagnetic transition operators in the IBM are written as the most general one-body operators with the required angular momentum. For example, the quadrupole transition operator, $T^{(2)}$, is given by [17]:

$$T^{(2)} = e_b (d^\dagger s + s^\dagger \tilde{d} + \chi (d^\dagger \tilde{d})^{(2)}) \tag{1.13}$$

where the parameters e_b, χ are determined by fitting the transitions to experimental data. The total transition probability between two states $|i L\rangle$ and $|i' L'\rangle$ with definite angular momentum L and L' , governed by the operator

$T^{(\lambda)}$, is given by:

$$B(T\lambda; iL \rightarrow i'L') \equiv \sum_{\mu, M'} |\langle i'L'M' | T_{\mu}^{(\lambda)} | iLM \rangle|^2 = \quad (1.14)$$

$$(2L+1)^{-1} |\langle i'L' || T^{(\lambda)} || iL \rangle|^2$$

where $\langle i'L' || T^{(\lambda)} || iL \rangle$ is the reduced matrix element, and is independent of M, M', μ .

When two intrinsic states with a definite angular momentum projection, K, K' and no definite angular momentum are given: $|\alpha K\rangle = \sum_L C_L |\alpha K L\rangle$, $|\alpha' K'\rangle = \sum_L C_L |\alpha' K' L\rangle$, it is sometimes needed to calculate the transition probability of the L -projected (normalized) states $|\alpha K L\rangle, |\alpha' K' L\rangle$. In such cases the reduced matrix element can be calculated as

$$(2L+1)^{-1/2} \langle \alpha' K' L' || T^{(\lambda)} || \alpha K L \rangle = \quad (1.15)$$

$$\frac{\sum_{\mu} (LK \lambda \mu | L', K + \mu) \int d\tau d_{K'K+\mu}^{(L')*}(\theta) \langle \alpha' K' | R(\theta) T_{\mu}^{(\lambda)} | \alpha K \rangle}{(\langle \alpha' K' | \int d\tau d_{K'K'}^{(L')*}(\theta) R(\theta) | \alpha' K' \rangle \langle \alpha K | \int d\tau d_{KK}^{(L)*}(\theta) R(\theta) | \alpha K \rangle)^{1/2}}$$

$$d_{K'K}^{(L)}(\theta) \equiv \langle LK' | e^{-i\theta \hat{L}_y} | LK \rangle \quad (\text{reduced Wigner-D matrix})$$

where $R(\theta) = e^{-i\theta \hat{L}_y}$ is the rotation operator, $d\tau = d(\cos \theta)$ and $\theta \in [0, \pi]$. Using this relation and Eq. (1.14), the total transition probability between these states can be written as

$$B(T\lambda; \alpha K L \rightarrow \alpha' K' L') = \quad (1.16)$$

$$\frac{|\sum_{\mu} (LK \lambda \mu | l', K + \mu) \int d\tau d_{K'K+\mu}^{(L')*}(\theta) \langle \alpha' K' | R(\theta) T_{\mu}^{(\lambda)} | \alpha K \rangle|^2}{\langle \alpha' K' | \int d\tau d_{K'K'}^{(L')*}(\theta) R(\theta) | \alpha' K' \rangle \langle \alpha K | \int d\tau d_{KK}^{(L)*}(\theta) R(\theta) | \alpha K \rangle}$$

If the L -projected states are written as a combination of n and n' states:

$$|\alpha K L\rangle = \sum_{i=1}^n f_i |\alpha_i K L\rangle \quad |\alpha' K' L'\rangle = \sum_{i=1}^{n'} g_i |\alpha'_i K' L'\rangle \quad (1.17)$$

then the transition probability in Eq. (1.14) is written as a combination of

the terms

$$B(T\lambda; \alpha KL \rightarrow \alpha' K' L') = \left| \sum_{i,j} f_i g_j^* (\langle \alpha' K' L' || T^{(\lambda)} || \alpha KL \rangle (2L+1)^{-1/2}) \right|^2 \quad (1.18)$$

where each term in the parenthesis is the same as in Eq. (1.15).

1.5 Partial Dynamical Symmetries

The concept of dynamical symmetry (Section 1.1) provides considerable insight, as it allows to find analytic solutions for the eigenstates and energies. In most cases, however, an Hamiltonian with an exact dynamical symmetry does not provide a good enough description of a nucleus, and other terms need to be added. *Partial dynamical symmetry* (PDS) [24] refers to a system in which the Hamiltonian does not have an exact dynamical symmetry, but still some symmetry properties remain. Partiality can be divided into three types:

- Type I: some of the eigenstates have all of the dynamical symmetry
- Type II: all of the eigenstates have part of the dynamical symmetry
- Type III: some of the eigenstates have part of the dynamical symmetry

A detailed discussion is given in [24] along with some algorithms to build different Hamiltonians which present these types of PDS. Two examples of PDS can be given when the Hamiltonian is chosen to be the intrinsic Hamiltonian of Eq. (1.12). An $SU(3)$ -PDS Type I [25–27] is obtained when setting $\beta_0 = \sqrt{2}$. If $h_0 = h_2$ then this Hamiltonian is an $SU(3)$ scalar. When $h_0 \neq h_2$, then the Hamiltonian is not an $SU(3)$ scalar, nevertheless there is a set of solvable states with good $SU(3)$ labels. These are the states projected from the condensate $|\beta_0 = \sqrt{2}, \gamma_0 = 0; N\rangle$. This condensate is a lowest weight vector of the $SU(3)$ irrep ($\lambda = 2N, \mu = 0$), and the states projected

from it by an $SO(3)$ projection, $[[N](2N, 0)K = 0 L\rangle$ with $L = 0, 2, \dots, 2N$, are eigenstates of the Hamiltonian with zero energy. A second example for a PDS is an $SO(6)$ -PDS Type III [28, 29] obtained by using the intrinsic Hamiltonian when setting $\beta_0 = 1$. Here, for $h_2 \neq 0$, the Hamiltonian is not an $SO(6)$ scalar, but a set of zero-energy eigenstates $[[N]\langle\sigma = N\rangle L\rangle$ ($L = 0, 2, \dots, 2N$) with mixed (τ) exists. These states can be projected from the intrinsic state with $\beta_0 = 1$, which is a lowest weight vector of the $SO(6)$ irrep with $\langle\sigma = N\rangle$.

Chapter 2

Quantum Shape Phase Transitions

As mentioned above, any IBM Hamiltonian can be associated with an equilibrium shape. This shape is defined by the values of the intrinsic variables β and γ at the global minimum of the energy surface.

Quantum shape phase transitions take place in the IBM when the equilibrium shape is changed as a function of a coupling constant in the Hamiltonian. The general procedure [30] consists of writing the Hamiltonian as a function of a coupling constant λ : $H = H(\lambda)$, followed by finding the minimum value for the energy surface (and equilibrium values β_0, γ_0) for each λ :

$$\begin{aligned} E^N(\beta, \gamma; \lambda) &= \langle \beta, \gamma; N | H(\lambda) | \beta, \gamma; N \rangle \\ E_{min}^N &= E^N(\beta_0(\lambda), \gamma_0(\lambda); \lambda) \end{aligned} \tag{2.1}$$

A first order phase transition is characterized by a discontinuity in the first derivative of E_{min}^N as a function of λ . This is clearly the case when the global minimum of the energy surface is changed abruptly as a function of λ . When this happens, then there exist a value of $\lambda = \lambda_c$, for which the energy surface has two coexisting global minima (see Figure 2.1).

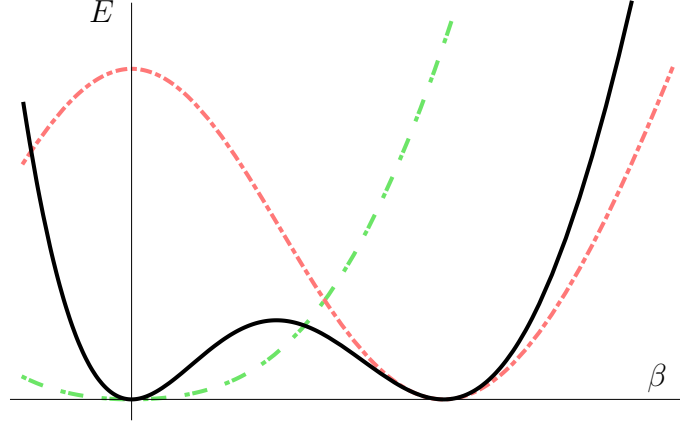


Figure 2.1: Energy surface in arbitrary units for a first-order phase transition. Each surface corresponds to a different value of λ . The solid line depicts the energy surface with two degenerate minima

2.1 2-Body IBM Hamiltonian

The general two-body IBM Hamiltonian was written in Eq. (1.1). The accompanied energy surface is [16]:

$$E(\beta, \gamma) = E_0 + N(N-1)\beta^2 \frac{[a - b\beta \cos 3\gamma + c\beta^2]}{(1 + \beta^2)^2}, \quad c > 0 \quad (2.2)$$

Here a, b, c are combinations of the parameters of the two-body Hamiltonian, and $c > 0$ is required for a physical Hamiltonian. The possible coexistence of global minima for the energy surface can only be achieved for spherical ($\beta = 0$) and axially-deformed shapes ($\beta = \beta_0, \gamma = 0$ or $\pi/3$), there cannot be two isolated deformed global minima in the two-body energy surface. In terms of the annihilation operators, the Hamiltonian that satisfies this coexistence can be built by using the $P_2^\dagger(\beta_0)$ operator. The energy surface then takes the form of Eq. (1.11).

2.2 3-Body IBM Hamiltonian

Up to this point only two-body interactions were considered. The main limitation that was stressed in the above sections, was the inability to construct an Hamiltonian that can accommodate two deformed degenerate minima. This prevented the IBM Hamiltonian from describing first order phase transition between two deformed shapes, and prevented the IBM from modeling the experimental results of deformed-deformed coexistence. This is not the case with the three-body IBM. The most general three-body IBM Hamiltonian can be written as [11]:

$$\begin{aligned}
H = & \sum_{L=0,2,3,4,6} r_L G_L^\dagger \cdot \tilde{G}_L + \sum_{L=0,2,4} [e_L(G_L^\dagger \cdot \tilde{K}_L + h.c.) + p_L K_L^\dagger \cdot \tilde{K}_L] \\
& + t_2(G_2^\dagger \cdot \tilde{d}s^2 + h.c.) + f_0(G_0^\dagger s^3 + h.c.) + w_2(K_2^\dagger \cdot \tilde{d}s^2 + h.c.) + x_0(K_0^\dagger s^3 + h.c.) \\
& + y_2(s^\dagger)^2 d^\dagger \cdot \tilde{d}s^2 + z_0(s^\dagger)^3 s^3
\end{aligned} \tag{2.3}$$

where $K_L^\dagger \equiv s^\dagger (d^\dagger d^\dagger)^{(L)}$, $G_L^\dagger \equiv [(d^\dagger d^\dagger)^{(\rho)} d^\dagger]^{(L)}$ and $(\rho, L) = (2, 0), (0, 2), (2, 3), (2, 4), (4, 6)$. The energy surface can be written as

$$\begin{aligned}
E(\beta, \gamma) &= N(N-1)(N-2)[z_0 + \tilde{E}(\beta, \gamma)] \\
\tilde{E}(\beta, \gamma) &= (1 + \beta^2)^{-3} \beta^2 (A\beta^4 + B\beta^4 \Gamma^2 + C\beta^3 \Gamma + D\beta^2 + E\beta \Gamma + F)
\end{aligned} \tag{2.4}$$

where $\Gamma = \cos(3\gamma)$ and A, B, C, D, E, F depend on the former 17 parameters.

For the proper choice of coefficients A, B, C, D, E, F , the three-body energy surface can have a degenerate deformed global minima or a triaxial one [11]. As a consequence, first order deformed-deformed phase transition can be modeled. The non-trivial question that remains is how to construct an appropriate three-body Hamiltonian, with an energy surface that contains two deformed global minima.

Chapter 3

Constructing the Critical Hamiltonian

As mentioned in Section 2.1, the two-body energy surface does not allow coexistence of doubly deformed shapes. By analyzing the general energy surface of a three-body Hamiltonian, it was shown [11] that the three-body IBM Hamiltonian can accomplish this goal. However, this Hamiltonian has 17 independent interactions. To find the interactions that are relevant for such coexistence, and can accommodate two deformed shapes, a selection criteria is needed. In the following section, we show how to construct a three-body *critical Hamiltonian* that allows for two degenerate prolate-prolate or prolate-oblate minima to coexist.

To find such Hamiltonian, the Hamiltonian will first be split into its intrinsic and collective parts, as was shown in Section 1.3: $H = H_{int} + H_{col}$. The intrinsic Hamiltonian for a double coexistence should satisfy Eq. (1.8) for two different condensates:

$$H_{int}|\beta_1, \gamma = 0; N\rangle = 0 \quad (3.1a)$$

$$H_{int}|\beta_2, \gamma = 0; N\rangle = 0 \quad (3.1b)$$

$$|\beta_i, 0; N\rangle \propto (s^\dagger + \beta_i d_0^\dagger)^N |0\rangle$$

These requirements automatically ensure that the energy surface of H will have two global minima at $\beta = \{\beta_1, \beta_2\}$ and $\gamma = 0$. Finding H_{int} then allows us to identify the three-body interactions that are important for the phase coexistence and to build a critical Hamiltonian.

In order to build the required intrinsic Hamiltonian, we will find operators \tilde{R}_L that annihilate the condensates. This is similar to Eq. (1.9), but instead of using the condition that the operators nullify the $|\beta_0, 0; N\rangle$ state, Eq. (3.1) will be translated into two equations on the operators. That is, we are looking for an operator \tilde{R}_L with a definite angular momentum L , so that

$$\begin{aligned}\tilde{R}_{L\mu}|\beta_1, 0; N\rangle &= 0 \\ \tilde{R}_{L\mu}|\beta_2, 0; N\rangle &= 0\end{aligned}\tag{3.2}$$

If such operators are found, then a scalar, N -conserving semi-positive definite Hamiltonian can be formed by

$$H_{int} = \sum_L h_L R_L^\dagger \cdot \tilde{R}_L\tag{3.3}$$

with $h_L > 0$. To find the possible \tilde{R}_L , we begin by listing the independent three-boson operators with definite L :

$$\begin{aligned}L = 0 : & \quad sss, \quad s(\tilde{d}\tilde{d})^{(0)}, \quad ((\tilde{d}\tilde{d})^{(2)}d)^{(0)} \\ L = 2 : & \quad ss\tilde{d}_\mu, \quad s(\tilde{d}\tilde{d})_\mu^{(2)}, \quad \tilde{d}(\tilde{d}\tilde{d})^{(0)} \\ L = 3 : & \quad [(\tilde{d}\tilde{d})^{(2)}\tilde{d}]_\mu^{(3)} \\ L = 4 : & \quad [(\tilde{d}\tilde{d})^{(2)}\tilde{d}]_\mu^{(4)}, \quad s(\tilde{d}\tilde{d})_\mu^{(4)} \\ L = 6 : & \quad [(\tilde{d}\tilde{d})^{(4)}\tilde{d}]_\mu^{(6)}\end{aligned}\tag{3.4}$$

Some of the operators are not listed since they depend on others. For example $[(\tilde{d}\tilde{d})^{(4)}\tilde{d}]^{(4)} = \sqrt{10/11}[(\tilde{d}\tilde{d})^{(2)}\tilde{d}]^{(4)}$. To build the required annihilation operators we try to construct an operator with a definite angular momentum, such that the two ‘‘annihilation equations’’ in (3.2) are satisfied. For the new operator to satisfy both equations for arbitrary β_1, β_2 (but not identically for

all β), we need at least three parameters (two equations and scaling). This is the case only for the operators with the angular momentum of zero and two. We found that there is a solution for both angular momenta. It is also noted that the operator with $L = 3$ annihilates the condensate $|\beta, 0; N\rangle$ for any β .

As an example for the calculation of Equation (3.2), the $L = 0$ operator $R_0(\beta_1, \beta_2)$ will be found. It is noted that when combining the three-body operators of Eq. (3.4), only the terms with triplets of $\{d_0, s\}$ needs to be considered - that is $d_0^2 s, s^3$ and d_0^3 . The other terms will annihilate the condensate regardless of the coefficients chosen. If R_0 exists, it can be written as $R_0 = x_1([\tilde{d}\tilde{d}]^{(2)}\tilde{d})^{(0)} + x_2(\tilde{d}\tilde{d})^{(0)}s^\dagger + x_3(s^\dagger)^3$, where the x_i are yet to be determined. Applying the operator on a condensate we find:

$$\begin{aligned} R_0|\beta_i, 0; N\rangle &\propto \left(x_1([\tilde{d}\tilde{d}]^{(2)}\tilde{d})^{(0)} + x_2(\tilde{d}\tilde{d})^{(0)}s^\dagger + x_3(s^\dagger)^3\right)|\beta_i, 0; N\rangle \\ &= [(2,0; 2,0|20)(2,0; 2,0|00)x_1d_0^3 + (2,0; 2,0|00)x_2d_0^2s + x_3s^3](s^\dagger + \beta_id_0^\dagger)^N|0\rangle \\ &= (-\sqrt{2/7}/\sqrt{5}x_1\beta_i^3 + 1/\sqrt{5}x_2\beta_i^2 + x_3)(\beta_is^\dagger + d_0^\dagger)^{N-3}|0\rangle \stackrel{!}{=} 0 \end{aligned} \quad (3.5)$$

Requiring that this equation holds for the two states $|\beta_i, 0; N\rangle$ ($i = 1, 2$), these conditions then become two equations in the x_i . In a similar manner the $L = 2$ operator $\tilde{R}_2(\beta_1, \beta_2)$ can be calculated. The two operators read:

$$\begin{aligned} R_0(\beta_1, \beta_2) &= x_1([\tilde{d}\tilde{d}]^{(2)}\tilde{d})^{(0)} + x_2(\tilde{d}\tilde{d})^{(0)}s + x_3(s)^3 \\ x_2 &= \sqrt{\frac{2}{7}}x_1\frac{\beta_1^2 + \beta_1\beta_2 + \beta_2^2}{\beta_1 + \beta_2} \quad x_3 = -\sqrt{\frac{2}{35}}x_1\frac{\beta_1^2\beta_2^2}{\beta_1 + \beta_2} \end{aligned} \quad (3.6)$$

and

$$\begin{aligned} \tilde{R}_2(\beta_1, \beta_2) &= \tilde{x}_1(\tilde{d}\tilde{d})^{(0)}\tilde{d} + \tilde{x}_2(\tilde{d}\tilde{d})^{(2)}s + \tilde{x}_3s^2\tilde{d} \\ \tilde{x}_1 &= \sqrt{\frac{10}{7}}\tilde{x}_2\frac{1}{\beta_1 + \beta_2} \quad \tilde{x}_3 = \tilde{x}_2\sqrt{\frac{2}{7}}\frac{\beta_1\beta_2}{\beta_1 + \beta_2} \end{aligned} \quad (3.7)$$

where the x_1, \tilde{x}_2 are scaling parameters.

The above results can now be used to build the intrinsic part of the critical

three-body Hamiltonian:

$$H_{int} = h_0 R_0^\dagger(\beta_1, \beta_2) R_0(\beta_1, \beta_2) + h_2 R_2^\dagger(\beta_1, \beta_2) \cdot \tilde{R}_2(\beta_1, \beta_2) \quad (3.8)$$

It is interesting to note that using Eq. (3.8) with arbitrary coefficients h_0, h_2 , there are other states, beside the two condensates, that are eigenstates with zero energy. These are the set of states in the $U(5)$ basis, labeled by $N = n_d = \tau, n_\Delta = 0$. To explain this, each of the constituents of R_0 and \tilde{R}_2 (Eqs. (3.6)-(3.7)) is regarded separately. We note that the states labeled by $n_d = N$ have no s^\dagger bosons, so that all the operators that contains s annihilates them. In addition $\tilde{d} \cdot \tilde{d}$ annihilates states labeled by $n_d = \tau$, because there are no d -boson pairs coupled to zero [17]. The last term that needs to be addressed is $([\tilde{d}\tilde{d}]^{(2)}\tilde{d})^{(0)}$. This operator annihilates all the $U(5)$ states labeled by $n_d = \tau, n_\Delta = 0, L = \tau, \tau + 1, ..2\tau - 2, 2\tau$ [24]. When all of the above conditions are united, then the states with $N = n_d = \tau, n_\Delta = 0, L = \tau, \tau + 1, ..2\tau - 2, 2\tau$ are annihilated by the six operators which compound R_0 and \tilde{R}_2 , for any values of the x_i 's.

It is also possible to express $R_0(\beta_1, \beta_2)$ and $\tilde{R}_2(\beta_1, \beta_2)$ in terms of the two-body annihilation operators $P_0(\beta_1)$ and $\tilde{P}_2(\beta_1)$ (see Section 1.3), coupled to either s or \tilde{d} bosons. This kind of operator will, by construction, annihilate the condensate $|\beta_1, 0; N\rangle$. It is then possible to set the ratio between the different operators so that it will annihilate the $|\beta_2, 0; N\rangle$ condensate as well. In terms of the scaling parameters x_1, \tilde{x}_2 of Eqs. (3.6),(3.7) the operators can be written as

$$\begin{aligned} R_0^\dagger &= a_1 s^\dagger P_0^\dagger(\beta_1) + a_2 P_2^\dagger(\beta_1) \cdot d^\dagger \\ a_2 &= x_1 / \sqrt{35}, \quad a_1 = \sqrt{\frac{2}{35}} x_1 \frac{\beta_2^2}{\beta_1 + \beta_2} \end{aligned} \quad (3.9)$$

and

$$\begin{aligned}
 R_2^\dagger &= b_1 d^\dagger P_0^\dagger(\beta_1) + b_2 (P_2^\dagger(\beta_1) d^\dagger)^{(2)} \\
 b_2 &= \tilde{x}_2 / (\sqrt{2}\beta_1), \quad b_1 = -\tilde{x}_2 \sqrt{\frac{2}{7}} \frac{\beta_2}{\beta_1} \frac{1}{\beta_1 + \beta_2}
 \end{aligned} \tag{3.10}$$

From first glance it appears that the R_2^\dagger operator has more freedom, as we can also use the $P_2^\dagger(\beta_1) s^\dagger$ operator, but this is not the case since the three operators $d^\dagger P_0^\dagger(\beta_1)$, $P_2^\dagger(\beta_1) s^\dagger$, $(P_2^\dagger(\beta_1) d^\dagger)^{(2)}$ are not independent:

$$(P_2^\dagger d^\dagger)_\mu^{(2)} = \frac{2}{\sqrt{7}} P_0^\dagger d_\mu^\dagger + \sqrt{\frac{2}{7}} \beta_1 P_{2\mu}^\dagger s^\dagger \tag{3.11}$$

Chapter 4

Energy Surface of the Critical Hamiltonian

In the following sections the energy surface that corresponds with the critical Hamiltonian will be analyzed, the extrema points will be identified, and the *energy barrier* will be found. The energy barrier is defined as the minimum energy difference the system will have to pass (in the configuration space, here β, γ) between the two minima. In the classical sense this corresponds to the minimum energy needed from some external agent to move the system between the two minima.

The three-body energy surface was given in Eq. (2.4). It is a difficult task to find the most general conditions on $A, B, ..F$, so that the energy surface will have two coexisting global minima at $(\beta_i, 0)$, $i = 1, 2$. A different approach will be taken. The intrinsic Hamiltonian H_{int} was found in Eq. (3.8). When $h_0, h_2 > 0$, the energy surface of H_{int} already have the required two global minima. The energy surface of this interaction will now be discussed.

The extrema points of the energy surface satisfy $dE/d\beta = 0, dE/d\gamma = 0$, and to classify the extrema points, the Hessian should be calculated. In

terms of the coefficients $A, B, ..F$, the extrema equations read [11]:

$$\beta[C\beta^5\Gamma + 2(D - 3A - 3B\Gamma^2)\beta^4 + (3E - 5C)\beta^3\Gamma + 4(F - D)\beta^2 - 3E\beta\Gamma - 2F] = 0 \quad (4.1)$$

$$\beta^3 \sin 3\gamma(2B\beta^3\Gamma + C\beta^2 + E) = 0 \quad (4.2)$$

If $B \neq 0$ and Eq. (4.1) is not satisfied identically for the same values that satisfy Eq. (4.2), then for $0 < \gamma < \pi/3$ these two equations support one solution in β and γ . The rest of the extrema are along the line $\gamma = 0$ (or $\gamma = \pi/3$). The Hessian along this line is given in Appendix A. It is seen that $\beta = 0$ is always an extremum. An extensive use will be made of the equality $E(\beta, \pi/3) = E(-\beta, 0)$, mentioned at the end of Section 1.2.1.

We note that $A, B, ..F$ are functions of the 4 parameters $\beta_1, \beta_2, h_0, h_2$, and by definition $h_0, h_2 \geq 0$. The β_i however, can take negative values, which corresponds to a global minima at $\beta = -\beta_i, \gamma = \pi/3$ (an oblate shape).

4.1 Energy Surface of $R_0^\dagger R_0$

The zero angular-momentum annihilation operator was found to be

$$R_0(\beta_1, \beta_2; x_1) = x_1 \left[([\tilde{d}\tilde{d}]^{(2)}\tilde{d})^{(0)} + \sqrt{\frac{2}{7}} \frac{\beta_1^2 + \beta_1\beta_2 + \beta_2^2}{\beta_1 + \beta_2} (\tilde{d}\tilde{d})^{(0)}_s - \sqrt{\frac{2}{35}} \frac{\beta_1^2\beta_2^2}{\beta_1 + \beta_2} s^3 \right] \quad (4.3)$$

$R_0(\beta_1, \beta_2; x_1)$ is determined up to scaling and henceforth $x_1 = 1$ will be used. When no confusion is likely to arise, it will be abbreviated to R_0 . The corresponding energy surface is

$$E_0(\beta, \gamma; \beta_1, \beta_2) \equiv \langle \beta, \gamma; N | R_0^\dagger R_0 | \beta, \gamma; N \rangle \quad (4.4)$$

$$= N(N-1)(N-2) \frac{2(\beta_1^2\beta_2^2 - (\beta_1^2 + \beta_2\beta_1 + \beta_2^2)\beta^2 + (\beta_1 + \beta_2)\beta^3 \cos 3\gamma)^2}{35(1 + \beta^2)^3(\beta_1 + \beta_2)^2} \quad (4.5)$$

It is a positive semi-definite function, as is required. For $\gamma = 0$ it reduces to

$$E_0(\beta, 0; \beta_1, \beta_2) = N(N-1)(N-2) \frac{2(\beta - \beta_1)^2(\beta - \beta_2)^2(\beta - \beta_3)^2}{35(1 + \beta^2)^3(\beta_1 + \beta_2)^2} \quad (4.6)$$

$$\beta_3 = -\beta_1\beta_2/(\beta_1 + \beta_2)$$

The energy surface is in general a function of β_1 and β_2 , as such it seems to have different “topologies” that needs to be taken into account (for example $\beta_1 < 0 < \beta_2$ and $0 < \beta_1 < \beta_2$). However, the surface has some symmetries that allows us to restrict the values of the β_i 's to $0 < \beta_2 < \beta_1$. The rest of the cases can be understood by using these symmetries. The symmetries for the energy surface (4.4) are:

- It is symmetric with respect to $\beta_1 \leftrightarrow \beta_2$: $E_0(\beta, \gamma; \beta_1, \beta_2) = E_0(\beta, \gamma; \beta_2, \beta_1)$
- It is symmetric with respect to $\beta_1 \rightarrow \beta_3 = -\beta_1\beta_2/(\beta_1 + \beta_2)$. That is $E_0(\beta, \gamma; \beta_1, \beta_2) = E_0(\beta, \gamma; \beta_3, \beta_2)$
- Taking $\beta_1 \rightarrow -\beta_1, \beta_2 \rightarrow -\beta_2$ is the same as taking $\beta \rightarrow -\beta$, that is $E_0(-\beta, \gamma; \beta_1, \beta_2) = E_0(\beta, \gamma; -\beta_1, -\beta_2)$.

To find and classify the extrema points, we make use of the extrema equations (4.1)-(4.2), the hessian equations (Eq. (A.0.1), p. 64) and the known global minima of the surface for $\gamma = 0$ from Eq. (4.6). A contour plot of the energy surface with the extrema points is given in Fig. 4.1.

Recalling that each (β, γ) such that $E_0(\beta, \gamma) = 0$ corresponds to an eigenstate $|\beta, \gamma; N\rangle$ with zero eigenvalue (but not vice versa), it is interesting to look for other zeros in the (β, γ) plane. It is found that the energy surface consists of two separated trajectories for which $E_0(\beta, \gamma) = 0$. The first one connects the two points $(\beta_2, 0)$ and $(|\beta_3|, \pi/3)$ and the second one begins at $(\beta_1, 0)$ and continues to infinity. These trajectories are depicted in Fig. 4.1 by a dashed line.

The last result which is of interest to this section, is to find the energy barrier discussed above. It can be seen, from the “zero trajectory” that the

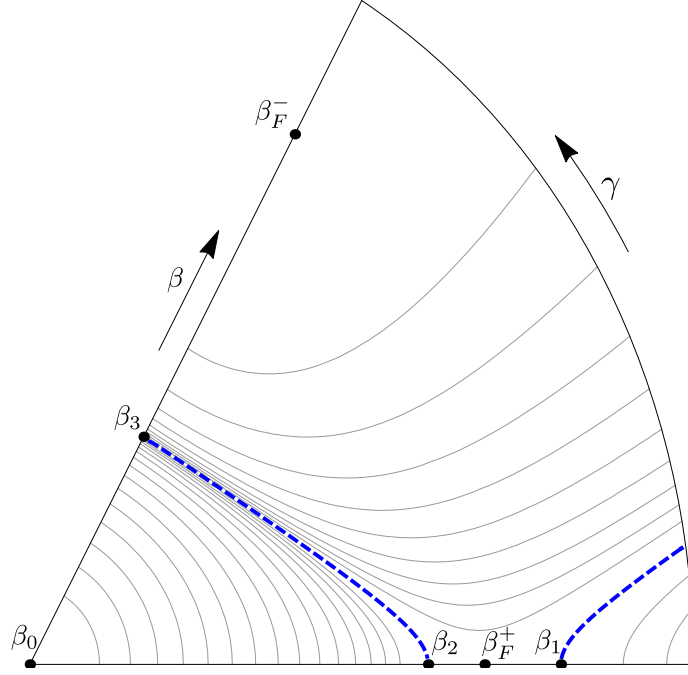


Figure 4.1: The $E_0(\beta, \gamma; \beta_1, \beta_2)$ energy surface. $\beta_1, \beta_2, \beta_3$ are global minima. β_F^-, β_0 are maxima, and β_F^+ is a saddle point. The dashed lines are the curves for which $E_0(\beta, \gamma; \beta_1, \beta_2) = 0$, and β_F^+ is the energy barrier between β_2, β_3 and β_1

barrier between β_2 and β_3 is zero. The barrier between β_1 and β_2 (or β_3) is the saddle point located at $(\beta_F^+, \gamma = 0)$. A detailed derivation of the above results is given in Appendix A.

The fact that the energy surface has trajectories in which it is zero, suggest that the intrinsic Hamiltonian $H = R_0^\dagger R_0$ cannot be used by itself to describe nuclei that exhibit phase coexistence. It must be accompanied by some other intrinsic operator that removes these zero-energy trajectories.

4.2 Energy Surface of $R_2^\dagger \cdot \tilde{R}_2$

The energy surface of this operator is found by calculating $E_2(\beta, \gamma; \beta_1, \beta_2) = \langle \beta, \gamma; N | R_2^\dagger \cdot \tilde{R}_2 | \beta, \gamma; N \rangle$ where \tilde{R}_2 is given in Equation (3.7). Setting $\tilde{x}_2 = 1$

the result is

$$E_2(\beta, \gamma; \beta_1, \beta_2) = N(N-1)(N-2) \times \frac{2\beta^2 \{ \beta^4 - 2(\beta_1 + \beta_2)(\beta^2 + \beta_1\beta_2)\beta \cos 3\gamma + (\beta_1^2 + 4\beta_2\beta_1 + \beta_2^2)\beta^2 + \beta_1^2\beta_2^2 \}}{7(1 + \beta^2)^3(\beta_1 + \beta_2)^2} \quad (4.7)$$

Setting $\gamma = 0$ the energy surface reduces to

$$E_2(\beta, 0; \beta_1, \beta_2) = N(N-1)(N-2) \frac{2\beta^2(\beta - \beta_1)^2(\beta - \beta_2)^2}{7(\beta^2 + 1)^3(\beta_1 + \beta_2)^2} \quad (4.8)$$

The energy surface has the symmetry $E_2(\beta, \gamma; \beta_1, \beta_2) = E_2(-\beta, \gamma; -\beta_1, -\beta_2)$, hence the analysis can be limited to the cases $\beta_1 > 0, \beta_2$ and $|\beta_2| < \beta_1$.

We note that setting $\beta = 0$ results in $E_2(0, \gamma) = 0$. This suggests that the state $|0, \gamma; N\rangle \propto (s^\dagger)^N |0\rangle$ is an eigenstate of the Hamiltonian $R_2^\dagger \cdot \tilde{R}_2$. An intrinsic state with $\beta = 0$ corresponds to a spherical shape.

In contrast to the $R_0^\dagger R_0$ energy surface, there are no other points in the $(\beta \neq 0, \gamma)$ plane beside the two points $(\beta_i, 0)$ or $(-\beta_i, \pi/3)$ (if $\beta_i < 0$) for which $E_2(\beta, \gamma) = 0$. This is evident from the fact that the energy surface is a monotonic function of γ , and is a non-negative function.

To find the other extrema of the energy surface we calculate:

$$\left. \frac{\partial E_2(\beta, \gamma)}{\partial \beta} \right|_{\gamma=0} = 0 \Rightarrow \frac{\beta(\beta - \beta_1)(\beta - \beta_2) \left\{ \beta^3(\beta_1 + \beta_2) + \beta^2(3 - 2\beta_1\beta_2) - 2\beta(\beta_1 + \beta_2) + \beta_1\beta_2 \right\}}{(1 + \beta^2)(\beta_1 + \beta_2)} = 0 \quad (4.9)$$

The three solutions to the expression in the curly braces, denoted by $\beta_1^m, \beta_2^m, \beta_3^m$ are maxima, and their locations can be solved exactly in terms of β_1, β_2 , as it is a cubic expression. Assuming $\beta_1 > 0, \beta_1 > |\beta_2|$ (the other cases can be found by the symmetry already discussed), the position of the three maxima

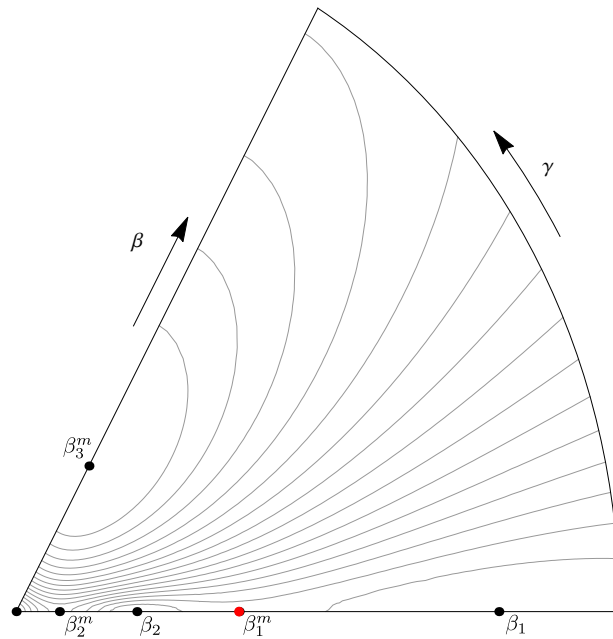
with respect to the global minima β_1 and β_2 is

$$\beta_3^m < 0 < \beta_2^m < \beta_2 < \beta_1^m < \beta_1 \quad (0 < \beta_2 < \beta_1) \quad (4.10a)$$

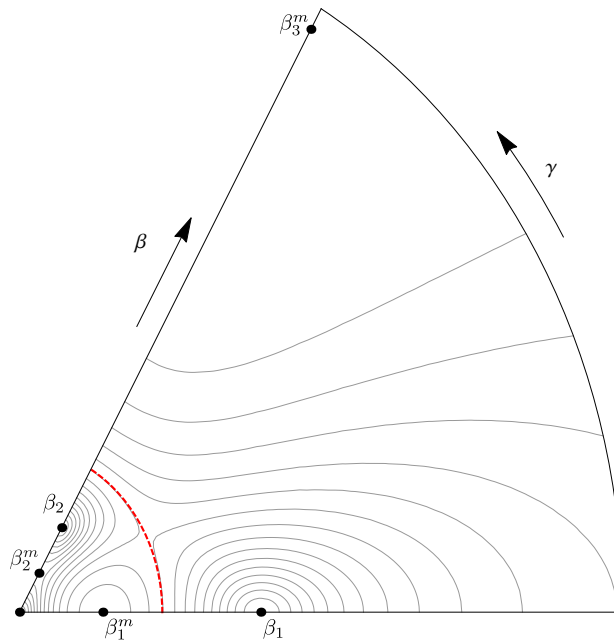
$$\beta_3^m < \beta_2 < \beta_2^m < 0 < \beta_1^m < \beta_1 \quad (\beta_2 < 0 < \beta_1, \beta_1 > |\beta_2|) \quad (4.10b)$$

To calculate the energy barrier as in the former section, the two cases should be treated separately. The barrier for the first case (4.10a) is the maximum between $(\beta_2, 0)$ and $(\beta_1, 0)$, and the location of the barrier for the second case, in Eq. (4.10b), is $\beta = \sqrt{|\beta_1\beta_2|}$ (arbitrary γ). The derivation of the above results is given in Appendix A.

Summarizing this section, the energy surface associated with the three-body operator $R_2^\dagger(\beta_1, \beta_2) \cdot \tilde{R}_2(\beta_1, \beta_2)$ was found and analyzed. It is depicted in Figure 4.2 on page 28. It was seen that the energy surface has a minimum at $\beta = 0$. As a consequence, this is the most general energy surface in the IBM (up to three-body interactions) that can describe a triple coexistence of two deformed (prolate or oblate) and spherical shapes. This coexistence was observed, for example in ^{186}Pb [6]. As a result, the three-body Hamiltonian $H = R_2^\dagger \cdot R_2$ is the most general intrinsic Hamiltonian that can be relevant for such nuclei.



(a) $\beta_1, \beta_2, 0$ are global minima. β_i^m are maxima. The barrier is located at β_1^m



(b) $\beta_1, \beta_2, 0$ are global minima. β_i^m are maxima. The dashed line represents the barrier and is an equipotential line

Figure 4.2: The two different topologies for the energy surface E_2 . $\beta_1 > \beta_2 > 0$ (top), and $\beta_1 > 0 > \beta_2, |\beta_2| < \beta_1$ (bottom)

4.3 Energy Surface of the Critical Hamiltonian

The complete intrinsic Hamiltonian is given by

$$H_{int} = h_0 R_0^\dagger R_0 + h_2 R_2^\dagger \cdot \tilde{R}_2 \quad (4.11)$$

and the energy surface of the critical Hamiltonian is given by

$$E(\beta, \gamma; \beta_1, \beta_2, h_0, h_2) = h_0 E_0(\beta, \gamma; \beta_1, \beta_2) + h_2 E_2(\beta, \gamma; \beta_1, \beta_2) \quad (4.12)$$

where E_0 and E_2 are given in Eqs. (4.4) and (4.7), $h_0, h_2 > 0$ and negative β_i corresponds, as always, to the point $(-\beta_i, \pi/3)$. The energy surface has a global minima only at $\beta = \beta_1$ and $\beta = \beta_2$, because the other minima of E_0 and E_2 do not coincide.

The other extrema of the energy surface depend on the four parameters $h_0, h_2, \beta_1, \beta_2$ in a complicated manner, and no attempt will be made to catalog them analytically. The energy surface for $\gamma = 0$ is

$$E(\beta, 0; \beta_1, \beta_2, h_0, h_2) = N(N-1)(N-2) \times \frac{2(\beta - \beta_1)^2(\beta - \beta_2)^2 \left\{ h_0(\beta_1\beta_2 + \beta(\beta_1 + \beta_2))^2 + 5h_2\beta^2 \right\}}{35(1 + \beta^2)^3(\beta_1 + \beta_2)^2} \quad (4.13)$$

and the energy value at infinity is

$$E_\infty \equiv E(\infty, 0; \beta_1, \beta_2) = N(N-1)(N-2) \left(\frac{2}{35} h_0 + \frac{2}{7} \frac{1}{(\beta_1 + \beta_2)^2} h_2 \right) \quad (4.14)$$

To find the energy barrier between the two minima, the prolate-prolate ($\beta_i > 0$, $i = 1, 2$) and prolate-oblate ($\beta_2 < 0 < \beta_1$) situations should be treated separately (the oblate-oblate surface is the same as that of the prolate-prolate with $\beta \rightarrow -\beta$). For the prolate-prolate energy surface, the barrier can be

found on the $\gamma = 0$ line between the two points. This is because for $\beta_2, \beta_1 > 0$, each of the combined energy surface is monotonically increasing in the γ variable. For the prolate-oblate energy surface, the barrier is located either at a saddle point with $0 < \gamma < \pi/3$ - this is always the case if the $\beta = 0$ point is maximum, or on the $\gamma = 0$ or $\gamma = \pi/3$ line.

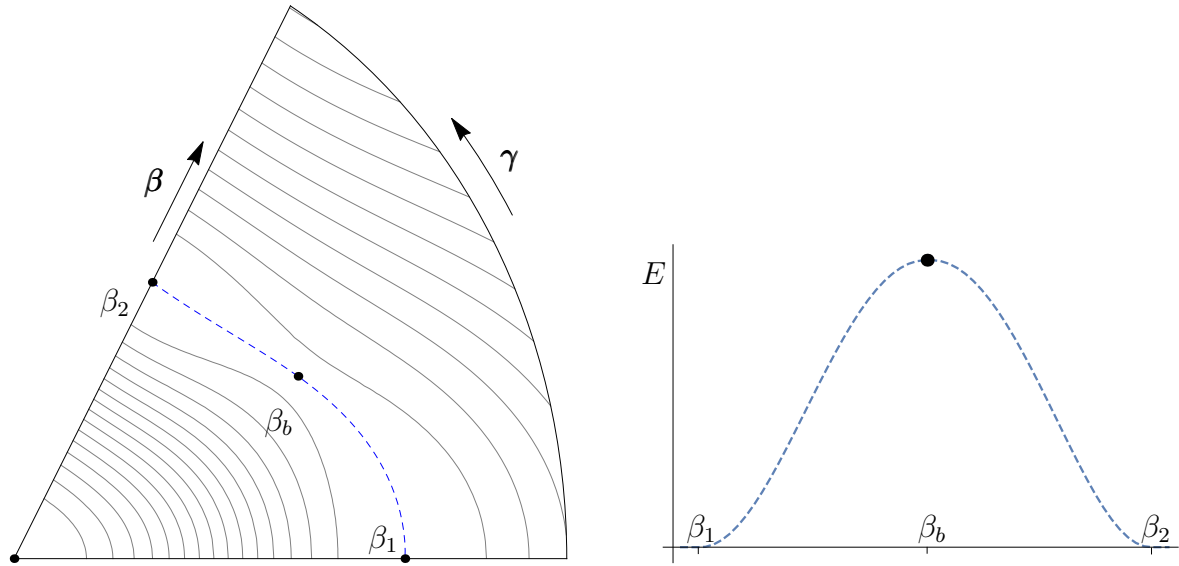
From numerical tests, it seems that the prolate-prolate energy barrier is usually lower than its prolate-oblate counterpart that is obtained by negating one of the β 's. Some values for the two barriers for different β_1, β_2 are given in Table 4.1.

	$E_{barrier}/E_\infty (10^{-2})$					
$ \beta_1 $	0.4	0.4	0.7	0.7	1	1
$ \beta_2 $	0.7	1	1	1.3	1.3	$\sqrt{2}$
prolate-oblate	0.331	1.981	0.887	4.11	1.24	2.406
prolate-prolate	0.008	0.153	0.01	0.155	0.09	0.03

Table 4.1: Energy barrier height, $E_{barrier}$, divided by the energy at infinity E_∞ from Eq. (4.14). The prolate-prolate and prolate-oblate are shown for different values of β_1, β_2 . The prolate-oblate values are obtained by using a negative value for β_2 . Here $h_0/h_2 = 1$

As a consequence, it seems that the more substantial barrier for the critical Hamiltonian is obtained for an oblate-prolate coexistence. Figure 4.3 shows an example for the energy surface of such Hamiltonian, along with a trajectory that connects the two minima and passes through the energy barrier.

To summarize, this section described the energy surface that is the result of the combined intrinsic Hamiltonian $H = h_0 R_0^\dagger R_0 + h_2 R_2^\dagger \cdot \tilde{R}_2$. It was explained that there are no more zeros in the energy surface, except the two required zeros. A numerical test seems to suggest that the energy barrier that corresponds with a prolate-oblate coexistence is generally higher than that of the prolate-prolate energy surface. In particular for all values that were tested, the barrier between a prolate-oblate energy surface and the prolate-prolate energy surface that is obtained by inverting the sign of the



(a) The energy barrier is located at the saddle point between the two points. There are two maxima: at $\beta = 0$ and β_3 (located outside of the figure on the $\gamma = \pi/3$ line). The dashed line shows a trajectory between the two minima that passes through the energy barrier.

(b) Energy (in arbitrary units) along the trajectory between the two β 's, depicted in dashed line in the left Figure.

Figure 4.3: The energy surface of the critical Hamiltonian with $\beta_1 = \sqrt{2}$, $\beta_2 = -1$ and $h_0/h_2 = 1$.

negative β_i , was found to be higher (as shown in Table 4.1). This seems to be in agreement with the empirical evidence that nuclei with prolate-oblate coexistence are more common than nuclei with prolate-prolate coexistence. Finally we have shown a contour plot for the energy surface of a prolate-oblate critical Hamiltonian.

4.4 Normal Modes Expansion of the Intrinsic Hamiltonian

The previous chapter had dealt only with the energy surface of the two three-body operators. This amounts to “classical” analysis of the Hamiltonian. No mention of eigenstates and eigenenergies was made.

In the following sections the two three-body operators will be explored with the concept of normal modes expansion (see Section 1.2.2).

If $R_0(\beta_1, \beta_2)$ and $\tilde{R}_2(\beta_1, \beta_2)$ are written in terms of the non-spherical basis, $b_i(\beta, \gamma)$ with $\beta = \beta_1$ or $\beta = \beta_2$ and $\gamma = 0$, then the two operators, by construction, will not include a b_c^3 component. This is a consequence of Eq. (3.2), and can in fact be used as a requirement to find these operators.

For large- N the condensate operators b_c^\dagger and b_c can be replaced with \sqrt{N} , as discussed in Section 1.2.2.

4.4.1 Normal Modes of $R_0^\dagger R_0$

Rewriting the $R_0^\dagger R_0$ operator, Eq. (4.3), with the GNSB, where $\beta = \beta_1$, $\gamma = 0$, $x_1 = 1$, replacing $b_c, b_c^\dagger \rightarrow \sqrt{N}$ and retaining the highest power of \sqrt{N} , we obtain

$$H_0^B(\beta_1, \gamma = 0) = \frac{2\beta_1^2(\beta_1 - \beta_2)^2(\beta_1 + 2\beta_2)^2}{35(1 + \beta_1^2)(\beta_1 + \beta_2)^2} N^2 b_\beta^\dagger b_\beta \quad (4.15)$$

where $b_\beta^\dagger \equiv b_\beta^\dagger(\beta_1, \gamma = 0)$ (this result is, of course, valid also for $\beta = \beta_2$ with $\beta_1 \leftrightarrow \beta_2$). It should be noted that there is no b_γ^\dagger dependency in the expression. This is in accordance with the fact that $\partial^2 E_0(\beta_1, \gamma)/\partial\gamma^2|_{\gamma=0} = 0$ in the corresponding energy surface (see Appendix A.1).

Along the zero-energy trajectory $E_0(\beta_t, \gamma_t) = 0$ (see Section 4.1) this

approximation yields

$$\begin{aligned}
H_0^B(\beta_t, \gamma_t) &= c_{\beta\beta} b_\beta^\dagger b_\beta + c_{\beta\gamma} [b_\gamma^\dagger b_\beta + h.c.] + c_{\gamma\gamma} b_\gamma^\dagger b_\gamma \\
c_{\beta\beta} &= N^2 \frac{2\Delta^2}{35\beta_t^2(1+\beta_t^2)^2(\beta_1+\beta_2)^2} & \Delta &= (3\beta_1^2\beta_2^2 - \beta_t^2(\beta_1^2 + \beta_1\beta_2 + \beta_2^2)) \\
c_{\beta\gamma} &= N^2 \frac{6\beta_t\Delta \sin(3\gamma_t)}{35(1+\beta_t^2)^{3/2}(\beta_1+\beta_2)} & c_{\gamma\gamma} &= N^2 \frac{18\beta_t^4 \sin(3\gamma_t)^2}{35(1+\beta_t^2)^2}
\end{aligned} \tag{4.16}$$

This expression can be written as two uncoupled number operators $H_0^B = \lambda_+ \omega_+^\dagger \omega_+ + \lambda_- \omega_-^\dagger \omega_-$. where λ_+, λ_- are found by diagonalizing the 2×2 Hermitian matrix c_{ij} ($i, j = \beta, \gamma$). The results are

$$\begin{aligned}
\lambda_+ &= N^2 \frac{2 \left\{ 9\beta_t^6(\beta_1 + \beta_2)^2 \sin^2(3\gamma_t) + (1 + \beta_t^2) (\beta_t^2 (\beta_1^2 + \beta_1\beta_2 + \beta_2^2) - 3\beta_1^2\beta_2^2) \right\}}{35\beta_t^2(1+\beta_t^2)^2(\beta_1+\beta_2)^2} \\
\lambda_- &= 0
\end{aligned} \tag{4.17}$$

Here again, the fact that one of the eigenvalues is zero is a consequence of the zero-energy trajectory. There is a direction in the (β, γ) plane in which the energy surface is constant.

To find the lower bands energies, we should, as noted above, use the normal modes expansion around the minima. However, it is unclear around which minima the Hamiltonian should be expanded, because (β_t, γ_t) consist of a continuous line in the (β, γ) plane.

The results above further strengthen the conclusions from Section 4.2 that $H = R_0^\dagger R_0$ cannot be used on its own to describe the intrinsic Hamiltonian for two degenerate deformed shapes.

4.4.2 Normal Modes of $R_2^\dagger \cdot R_2$

Rewriting the $R_2^\dagger \cdot \tilde{R}_2$ operator, Eq. (3.7), with the GNSB, where $\beta = \beta_1$, $\gamma = 0$, $\tilde{x}_2 = 1$, replacing $b_c^\dagger, b_c \rightarrow \sqrt{N}$ and retaining the highest \sqrt{N} power, the

result is

$$H_2^B(\beta_1, \gamma = 0) = \frac{2}{7} \left\{ \frac{\beta_1^2(\beta_1 - \beta_2)^2}{(1 + \beta_1^2)(\beta_1 + \beta_2)^2} b_\beta^\dagger b_\beta + \frac{9\beta_1^2}{(1 + \beta_1^2)^2} (b_z^\dagger b_z + b_\gamma^\dagger b_\gamma) \right\} N^2 \quad (4.18)$$

where $b_i^\dagger \equiv b_i^\dagger(\beta_1, \gamma = 0)$. In contrast to the former operator, here the $b_\gamma^\dagger b_\gamma$ term is not zero. This is because the two points $(\beta_1, 0)$ and $(\beta_2, 0)$ are not part of a continuous zero-energy trajectory.

We note that $b_z^\dagger b_z$ appears with the same coefficient as $b_\gamma^\dagger b_\gamma$. This is a consequence of the symmetry around the z -axis: z is not a Goldstone-mode (as opposed to the rotation around the x - or y - axes), and the γ -vibration is two dimensional [22].

4.4.3 Normal Modes Expansion of the Intrinsic Hamiltonian

The general three-body intrinsic Hamiltonian is composed of the two operators together: $H = h_0 R_0^\dagger R_0(\beta_1, \beta_2) + h_2 R_2^\dagger \cdot \tilde{R}_2(\beta_1, \beta_2)$. For $h_0, h_2 > 0$ there are two equilibrium points in the (β, γ) plane. These are the points $(|\beta_1|, \gamma_1)$ and $(|\beta_2|, \gamma_2)$, where $\gamma_i = 0$ ($\gamma_i = \pi/3$) for $\beta_i > 0$ ($\beta_i < 0$). Combining the results of the last two sections, the approximated energies can be written as:

$$E(n_1^\beta, n_2^\beta, n_1^\gamma, n_2^\gamma; \beta_1, \beta_2) = \epsilon_{1,\beta} n_1^\beta + \epsilon_{2,\beta} n_2^\beta + \epsilon_{1,\gamma} n_1^\gamma + \epsilon_{2,\gamma} n_2^\gamma \quad (4.19)$$

where

$$\begin{aligned} \epsilon_{1,\beta} &= N^2 \frac{2}{7} \frac{\beta_1^2(\beta_1 - \beta_2)^2}{(1 + \beta_1^2)(\beta_1 + \beta_2)^2} \left(\frac{h_0(\beta_1 + 2\beta_2)^2}{5} + h_2 \right) & \epsilon_{1,\gamma} &= N^2 \frac{18\beta_1^2}{7(1 + \beta_1^2)^2} h_2 \\ \epsilon_{2,\beta} &= N^2 \frac{2}{7} \frac{\beta_2^2(\beta_2 - \beta_1)^2}{(1 + \beta_2^2)(\beta_2 + \beta_1)^2} \left(\frac{h_0(\beta_2 + 2\beta_1)^2}{5} + h_2 \right) & \epsilon_{2,\gamma} &= N^2 \frac{18\beta_2^2}{7(1 + \beta_2^2)^2} h_2 \end{aligned} \quad (4.20)$$

N is the number of bosons, $n_j^i (j = 1, 2, i = \beta, \gamma)$ are the excitation-numbers around each equilibrium point and β or γ band.

We note that the ratio between the two γ -bands is independent of the coefficients h_0, h_2

$$\frac{\epsilon_{1,\gamma}}{\epsilon_{2,\gamma}} = \frac{(1 + \beta_2^2)^2 \beta_1^2}{(1 + \beta_1^2)^2 \beta_2^2} \quad (4.21)$$

and the ratio between the two β -bands is

$$\frac{\epsilon_{1,\beta}}{\epsilon_{2,\beta}} = \frac{(1 + \beta_2^2) \beta_1^2}{(1 + \beta_1^2) \beta_2^2} \left(\frac{(\beta_1 + 2\beta_2)^2 h_0 + 5h_2}{(\beta_2 + 2\beta_1)^2 h_0 + 5h_2} \right) \quad (4.22)$$

For the spherical-deformed-deformed case ($h_0 = 0$), the values β_i^2 are known once the ratios between the different bands, Eqs. (4.21) and (4.22), are known. For the solution of the β_i 's to be real, this restricts the possible ratios between the β and γ bands: If the bands are labeled so that $\epsilon_{2,\beta} > \epsilon_{1,\beta}$, then for a real solutions for the β_i 's, it must be that $\frac{\epsilon_{1,\gamma}}{\epsilon_{1,\beta}} > \frac{\epsilon_{2,\gamma}}{\epsilon_{2,\beta}}$

Chapter 5

Analysis of the Intrinsic Hamiltonian

The intrinsic part of the critical Hamiltonian with a coexistence of deformed-deformed shapes is $H_{int} = h_0 R_0^\dagger R_0 + h_2 R_2^\dagger \cdot \tilde{R}_2$ with arbitrary β_1, β_2 and $h_0, h_2 > 0$. It was stated at the previous section that the energy barrier of prolate-oblate nuclei is generally much higher than that of the prolate-prolate nuclei, in addition prolate-oblate nuclei are more common in heavy nuclei.

For these reasons, this chapter will focus on prolate-oblate intrinsic Hamiltonian. In order to facilitate the identification of bands, the values $\beta_1 = \sqrt{2}$, $\beta_2 = -1$ will be chosen. This ensures that each of the ground-bands can be identified with its corresponding minima, as the $\beta_1 = \sqrt{2}$ yields $SU(3)$ PDS and $\beta_2 = -1$ yields $SO(6)$ PDS (see Section 1.5). The excited states of each minima are expected to keep some of the PDS characteristics, and as such should also be easier to identify.

The spectrum of the critical Hamiltonian with $h_0 = h_2 = 1, \beta_1 = \sqrt{2}, \beta_2 = -1$ and $N = 20$ is shown in Figure 5.1. The eigenstates are clustered in groups of different energies. A zoom-in into the lowest group is shown in Fig. 5.2 (page 38), and a zoom-in into the second group is show in Fig. 5.3 (page 40).

Focusing on the lower group, the zero-energy states are doubly degenerate

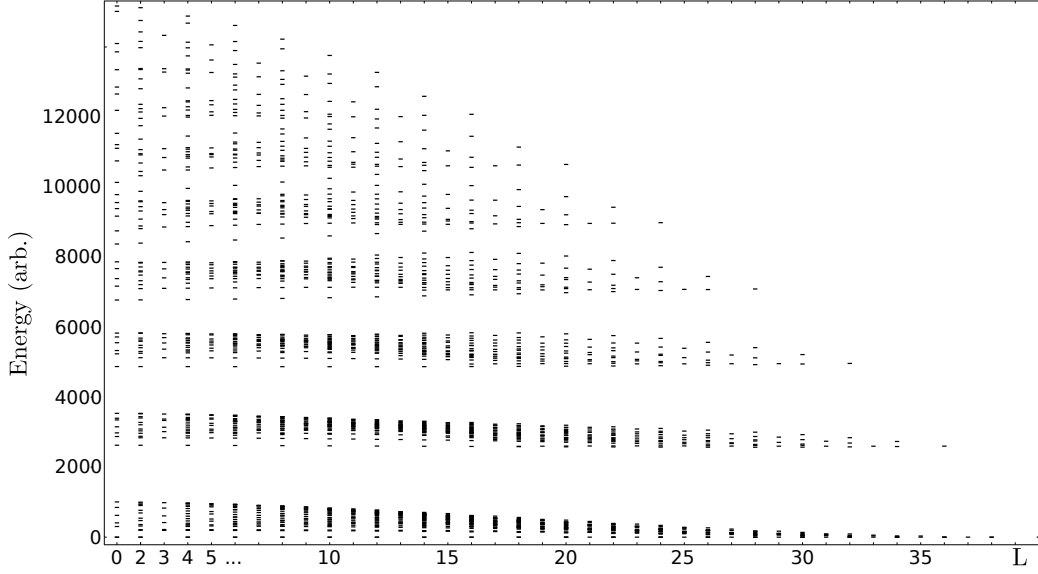


Figure 5.1: An energy plot for $\beta_1 = \sqrt{2}$, $\beta_2 = -1$, $N = 20$ and $h_0 = h_2 = 1$. The states are clustered in “groups” of different energies.

(for $L \leq 10$), as required from the construction of the Hamiltonian. The states with different angular momenta are seemed to be divided into almost degenerate bands. Specifically, the degenerate zero-energy states form two ground-bands and the first two excited bands (indicated by disk and plus-sign in Fig. 5.2) resembles γ -bands. The states with higher energies (indicated by stars), have the correct angular-momenta for the γ^2 -bands (with $K = 0, 4$).

The next group of states, depicted in Fig. 5.3 also seems to be composed of (almost) degenerate bands. The lowest states, indicated by a disk, and the states indicated by a star have even angular momentum, which resembles a $K = 0$ band (for example a β -band), while the states indicated by plus-sign have angular momenta $L = 2, 3, \dots$, and resembles a band with $K = 2$ (for example a γ - or $\beta\gamma$ - band).

To further test if these states can be considered a band, the inter- and intra- band transitions were calculated using the transition operator $T^{(2)}$ of Eq. (1.13) with $\chi = 0$. Some values for the transitions are given in Table 5.1 (page 39). It is seen that the ground-, γ - and β - bands intraband transitions are much stronger than the interband transitions. The transitions between

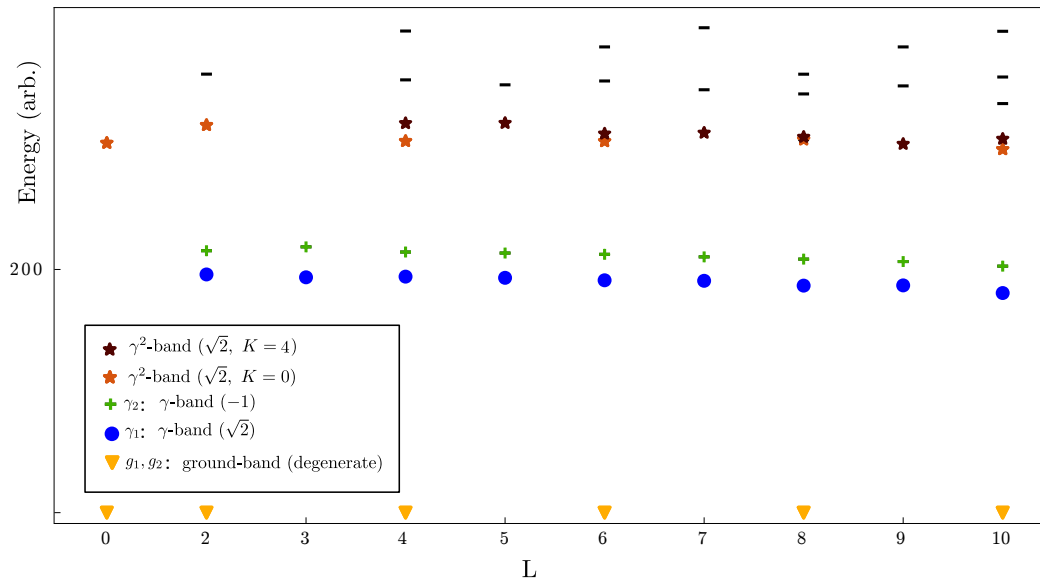


Figure 5.2: L-Energy plot for $N = 20$. This is a zoom-in on the lowest group of states from Fig. 5.1

the states in the γ^2 -bands (for clarity, these are marked as two separate bands, see Fig. 5.2), however, do not indicate a clear band structure of two bands. The Alaga rules were also computed for the transitions, Table 5.2 shows a comparison between some of the $E2$ transition-relations with the accompanied Alaga predictions. This further supports the notion bands-structure, as depicted earlier (Fig. 5.2 and Fig. 5.3).

	E2 Transitions					
	$6 \rightarrow 4$	$4 \rightarrow 2$	$2 \rightarrow 0$			
$g_1 \rightarrow g_1$	154.783	142.028	100			
$g_2 \rightarrow g_2$	174.588	160.010	112.586			
$\gamma_1 \rightarrow \gamma_1$	113.030	46.4573	–			
$\gamma_2 \rightarrow \gamma_2$	115.944	51.8093	–			
$\beta_1 \rightarrow \beta_1$	131.775	121.617	85.900			
$\beta_2 \rightarrow \beta_2$	145.025	130.303	91.338			
$\beta\gamma \rightarrow \beta\gamma$	90.9188	47.0475	–			
	$6 \rightarrow 4$	$4 \rightarrow 2$	$2 \rightarrow 0$	$6 \rightarrow 6$	$4 \rightarrow 4$	$2 \rightarrow 2$
$g_1 \rightarrow g_2$	0.0001	0.0001	0.0004	0	0	0.0001
$\gamma_2 \rightarrow g_2$	1.6673	2.4211	4.7641	8.8868	8.9700	7.5180
$\gamma_2 \rightarrow g_1$	0.0757	0.0735	0.1658	0.4567	0.3525	0.1592
$\gamma_2 \rightarrow \gamma_1$	0.0011	10.561	–	13.838	3.6977	23.108
$\beta_2 \rightarrow \beta\gamma$	0.4053	1.1401	–	0.6955	0.8142	0.1878
$\beta_2 \rightarrow \beta_1$	0	0.0018	0.0241	0.02	0.0278	0.0689
$\beta\gamma \rightarrow \beta_1$	1.4599	1.7620	2.9448	5.0638	5.0717	4.1974

Table 5.1: Some of the interband and intraband transitions. For the critical Hamiltonian. Here $N = 20$ and $\chi = 0$. The left column specify the bands and the upper row specify the angular momentum. It can be seen that the intraband transitions (upper half of the table) are stronger than the interband (lower half). The transitions are normalized by $2_1 \rightarrow 0_1 = 100$

E2 Transition Relations					
$K = 0$	g_1	g_2	β_1	β_2	Alaga
$\frac{6 \rightarrow 4}{4 \rightarrow 2}$	1.0898	1.0911	1.084	1.113	1.1014
$\frac{4 \rightarrow 2}{2 \rightarrow 0}$	1.4203	1.4212	1.4159	1.4266	1.4286
$K = 2$	γ_1	γ_2	$\gamma\beta$		Alaga
$\frac{6 \rightarrow 4}{4 \rightarrow 2}$	2.433	2.2379	1.932		1.9737

Table 5.2: Comparison of the $E2$ intraband transition relations with the corresponding Alaga values. For the upper table $K = 0$ and for the lower table $K = 2$. Here $\chi = 0$

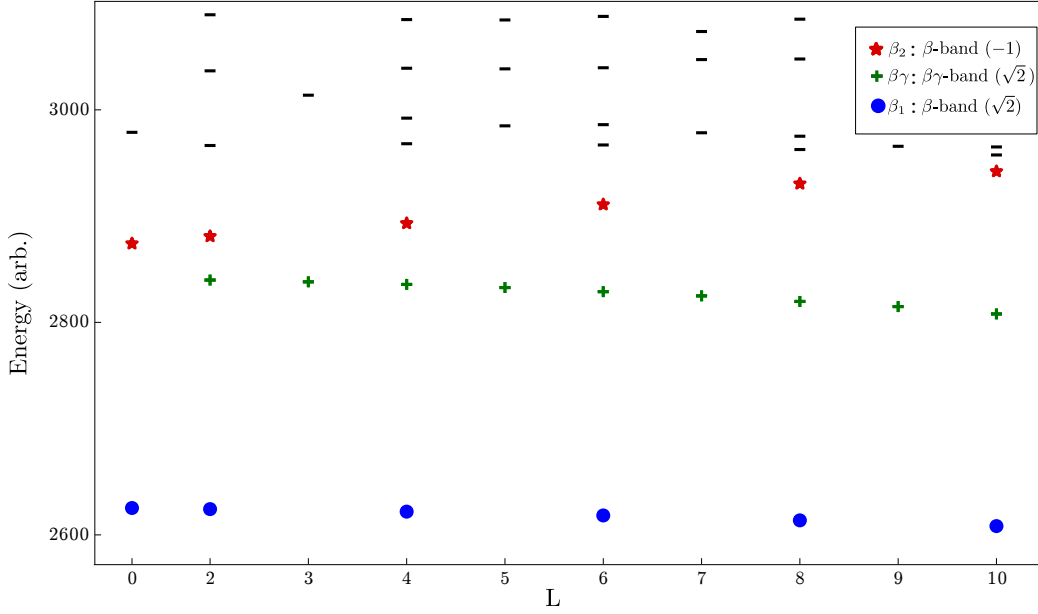


Figure 5.3: L-Energy plot for $N = 20$, this is a zoom-in into the second group of states from Fig. 5.1

5.1 Identification of the Bands

The normal modes expansion for the intrinsic three-body Hamiltonian were discussed in Section 4.4, and the energies for the bands were given in Eq. (4.19). Using the values $h_0 = h_2, \beta_1 = \sqrt{2}, \beta_2 = -1$ for the critical Hamiltonian, the normal modes energies are:

$$E(n_1^\beta, n_2^\beta, n_1^\gamma, n_2^\gamma; \beta_1 = \sqrt{2}, \beta_2 = -1) = N^2(6.91n_1^\beta + 8.10n_2^\beta + 0.57n_1^\gamma + 0.64n_2^\gamma) \quad (5.1)$$

We see that there is an order of magnitude difference between the β and γ coefficients. This can explain the groups of states discussed earlier (Fig. 5.1). The lower groups is composed of the states belonging to the ground and γ bands and their overtones: $\gamma_1\gamma_2, \gamma_1^2, \dots$ (Fig. 5.2). The next group is composed of the states belonging to the β -bands along with the γ overtones: $\beta_1, \beta_2, \beta_1\gamma_1, \dots$ (Fig. 5.3). The third group is composed of states with β^2 -bands and so on.

N	Energy/ N^2					E_{barrier}/N^2
	γ_1	γ_2	β_1	β_2	$\beta_1\gamma_1$	
10	0.40	0.51	6.03	—	—	0.30
15	0.45	0.51	6.41	6.86	6.95	0.50
20	0.48	0.54	6.56	7.19	7.10	0.71
25	0.51	0.56	6.66	7.38	7.20	0.91
29	0.52	0.57	6.69	7.50	7.24	1.08
34	0.53	0.59	6.73	7.57	7.29	1.29
40	0.53	0.60	6.76	7.66	7.32	1.54
$\epsilon_{i,j}$	0.57	0.64	6.91	8.10	7.49	

Table 5.3: Exact results for the energies of each band and each N (divided by N^2). This should be compared with the corresponding normal-mode coefficients, $\epsilon_{i,j}$, of Equation (4.19). The energies of the $\beta\gamma$ -band corresponds to $\epsilon_{1,\beta} + \epsilon_{1,\gamma}$ and the numerical energy is computed from the eigenstate with the lowest angular-momentum. The right-most column shows the value of the energy barrier of Section 4.3, divided by N^2 .

The approximated energies in Eq. (5.1) also helps to identify which γ and β bands belongs to which minima in the energy surface. Since the energies related with $\beta = \sqrt{2}$ are lower than those of $\beta = -1$, we associate the γ_1 and β_1 bands with the $\beta = \sqrt{2}$ minimum and the γ_2 and β_2 bands with $\beta = -1$ minimum. This association can be made for different N 's. The normal modes expansion should provide better approximation as N grows. A comparison of the exact and normal-mode energies for various N is given in Table 5.3.

To gain further insight into the bands structure and to affirm the association of the various bands with their corresponding minima, it is advantageous to decompose the various bands into the $SU(3)$ and $SO(6)$ dynamical-symmetry chains. As mentioned in Section 1.5, the condensate $|-1, 0; N\rangle$ has a good $\langle\sigma = N\rangle$ $SO(6)$ -label, and the condensate with $|\sqrt{2}, 0; N\rangle$ has a good $(\lambda = 2N, \mu = 0)$ $SU(3)$ -label. These condensates furnish the two ground-bands g_1 and g_2 with pure character. The decomposition of these bands into the $SO(6)$ and $SU(3)$ symmetries is shown in Fig. 5.4.

The decomposition of the two γ -bands is shown in Figures 5.5–5.6. It

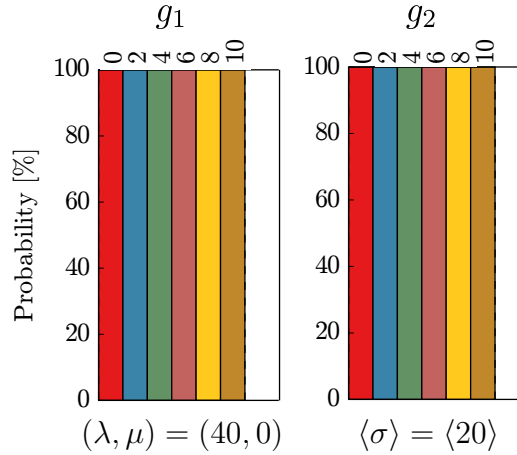


Figure 5.4: The decomposition of the two ground-bands. The left figure depicts the probability of the g_1 -band into the (λ, μ) irrep. The right figure depicts the probability of the g_2 -band into the $\langle \sigma \rangle$ irrep. Here $N = 20$, and the numbers $0, 2, 4, \dots$ are different angular momenta

can be seen that the γ_1 -band has a coherent decomposition in the $SU(3)$ basis, and a dominant $(\lambda = 36, \mu = 2)$ component. This is reflected in the corresponding intrinsic state, since in the large- N limit, the $SO(3)$ projected states of the β and γ intrinsic states of $\beta = \sqrt{2}$, defined in Eq. (1.7), have a good $(\lambda = 2N - 4, \mu = 2)$ label [22].

The γ_2 -band is coherent when decomposed into the the $SU(3)$ basis, which is again expected from states that belong to the same band. The decompo-

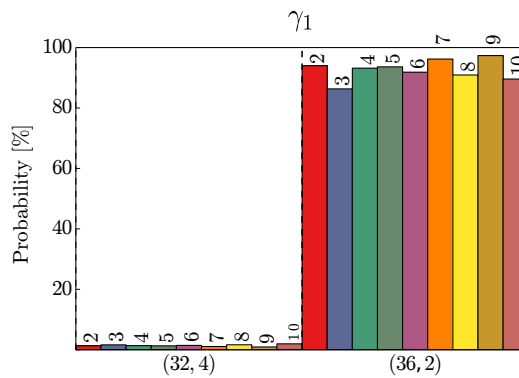


Figure 5.5: The probability of the γ_1 -band to be in the (λ, μ) sub-spaces. These are the states marked by disks in Fig. 5.2

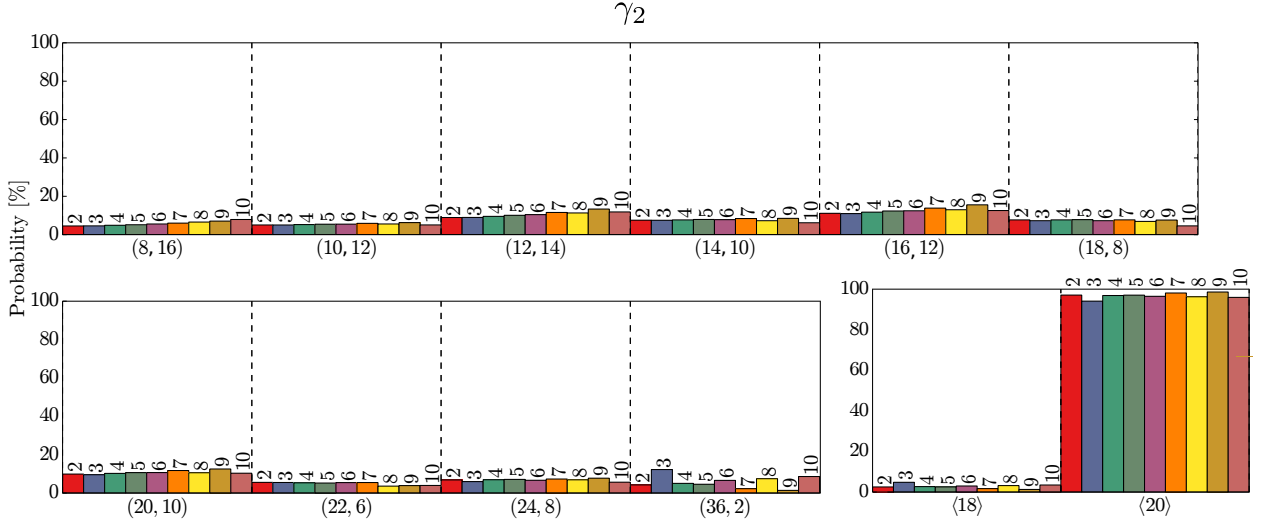


Figure 5.6: Probability of the γ_2 -band to be in the (λ, μ) sub-spaces of $SU(3)$ and $\langle \sigma \rangle$ sub-spaces of $SO(6)$.

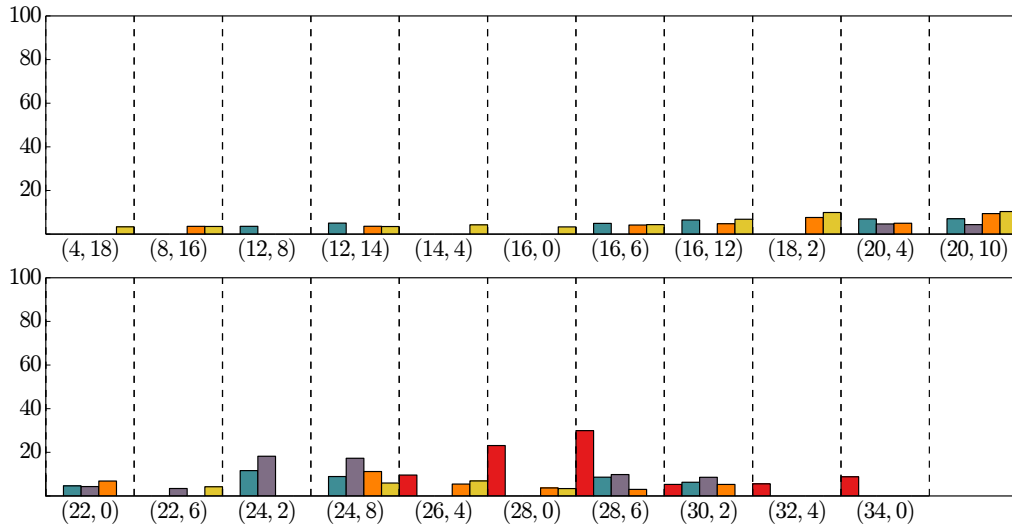
sition into the $SO(6)$ basis show that the states have dominant $\langle \sigma = 20 \rangle$ component. Again, this is reflected in the γ -band that corresponds with $\beta = -1$. These states have a probability of $(N - 1)/(N + 1)$ to be in the $\langle \sigma = N \rangle$ subspace, and a probability $2/(N + 1)$ to be in the $\langle \sigma = N - 2 \rangle$ subspace (see Appendix B).

A decomposition of the two β -bands can also be carried out. The dominant (λ, μ) component of the β_1 -band ($\beta = \sqrt{2}$) is $(36, 2)$ and has a probability of 89%-90%. It is mixed with the $(34, 0)$ component (8.3%-9.7%). This fits with the interpretation of the β_1 -band as being associated with the β -band that belongs to the $\beta = \sqrt{2}$ minimum. The decomposition of the β_2 -band into the $SO(6)$ symmetry shows that the states have a probability of 94%-96% to be in the $\langle \sigma = 18 \rangle$ subspace, and 0.3%-0.45% to be in the $\langle \sigma = 20 \rangle$ subspace, with the exception of the $L = 10$ state which is more strongly mixed and has an additional components of $\langle 10 \rangle$ with a probability of about 10%. Again, this corresponds with the states that are projected from the intrinsic β state associated with the $\beta = -1$ minimum. These states have a probability of $(N - 1)/(N + 1)$ to be in the $\langle \sigma = N - 2 \rangle$ subspace, and a probability of $2/(N + 1)$ to be in the $\langle \sigma = N \rangle$ subspace (see Appendix

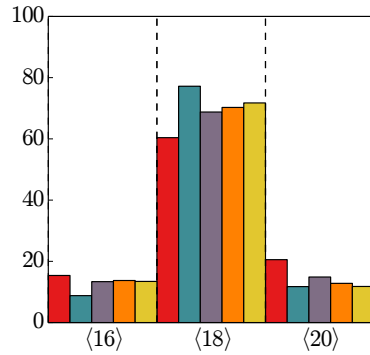
B). The $\beta\gamma$ -band is mainly composed of the $(32, 4)$ component (76%-80%) and the $(30, 2)$ components (17%-21%).

The intrinsic Hamiltonian, with the parameters $\beta_1 = \sqrt{2}$ and $\beta_2 = -1$ exhibits an interesting phenomena. This Hamiltonian provides a coexistence of two partial dynamical symmetries of two non-compatible chains, $SU(3)$ and $SO(6)$. The intrinsic state $|-1, 0; N\rangle$ provides an $SO(6)$ -PDS type III: the states projected from it have the $SO(6)$ $\langle\sigma = N\rangle$ label, but do not have a good (τ) label. The intrinsic state $|\sqrt{2}, 0; N\rangle$, on the other hand, provides an $SU(3)$ -PDS type I: the states projected from it have the $SU(3)$ $(\lambda = 2N, \mu = 0)$ label. The other eigenstates of the intrinsic Hamiltonian do not necessarily possess any of these symmetry labels. The decomposition of a few non-PDS states are shown in Fig. 5.7. This should be compared with the states from Fig. 5.4.

In this section we have inspected the spectrum and transitions of the intrinsic part of the three-body critical Hamiltonian with a prolate-oblate coexistence. This Hamiltonian, by construction, has two degenerate ground-bands. The spectrum of the Hamiltonian showed, beside the ground-bands, clear indications of two γ - and two β - bands. The transitions between the states were also calculated and showed further indications that these states can be considered as bands. We used the approximated energies from the normal modes expansion to identify the bands with their corresponding minima. We decomposed the wave-functions of the band members into the $SO(6)$ and $SU(3)$ dynamical symmetry basis to furthermore understand their structure. It was seen that the γ - and β - bands states are coherent and their decomposition is similar to that of the γ - and β - bands obtained by projection of the intrinsic excited states. Lastly, we have shown that for the specific values of β_1 and β_2 chosen for this section, the intrinsic Hamiltonian presents two PDS of different symmetries. This is a more complex situation than encountered with the two-body IBM (see Section 1.5), where the choice of β_0 can produce either $SU(3)$ -PDS or $SO(6)$ -PDS, but not both of them together.



(a) Decomposition into the $SU(3)$ (λ, μ) dominant components



(b) Decomposition into the $SO(6)$ $\langle \sigma \rangle$ dominant components

Figure 5.7: Decomposition of some eigenstates of the intrinsic Hamiltonian into dominant irreps of both the $SU(3)$ and $SO(6)$ symmetries. Different colors indicate different states. This should be compared with the states from Fig. 5.4

Chapter 6

Collective Terms for the Critical Hamiltonian

Up to this point only the intrinsic part of the critical Hamiltonian was considered. To continue further, we need to consider the kinetic terms, which do not affect the potential. In this section the collective operators will be added to the intrinsic critical Hamiltonian, and their affect on the spectrum and transitions will be analyzed. The collective operators we choose to employ are the three-body collective terms from [11]. The collective Hamiltonian can be written as

$$\begin{aligned} H_{col} = & c_3(N-2)(\hat{C}_{O(3)} - 6\hat{n}_d) + c_5(N-2)(\hat{C}_{O(5)} - 4\hat{n}_d) + \\ & c_6(N-2)(\hat{C}_{\overline{O(6)}} - 5N) + d_3(\hat{n}_d - 2)(\hat{C}_{O(3)} - 6\hat{n}_d) + \\ & d_5(\hat{n}_d - 2)(\hat{C}_{O(5)} - 4\hat{n}_d) + \\ & d_6[(\hat{n}_d - 1)(\hat{C}_{\overline{O(6)}} - 5N) - (\hat{C}_{O(5)} - 4\hat{n}_d) + h.c.] \end{aligned} \quad (6.1)$$

here c_i, d_i are parameters. The terms multiplied by c_i are the three-body parts of $\hat{N}\hat{C}_g$, $g = O(3), O(5), \overline{O(6)}$ and the terms multiplied by the d_i are proportional to the the three body parts of $\hat{n}_d C_g + h.c.$ The complete Hamil-

tonian, containing the intrinsic and collective terms takes the form

$$H = h_0 R_0^\dagger R_0 + h_2 R_2^\dagger \cdot \tilde{R}_2 + H_{col} \quad (6.2)$$

As a result of adding the collective terms, the two ground-bands will no longer be degenerate. The wave-functions, energies and inter- and intraband transitions of these states will change. In the following section, each of the collective terms is added separately to the critical Hamiltonian. Table 6.1 shows the energies of the critical Hamiltonian with the addition of the collective terms. The coefficient of the collective terms were chosen to be large enough to change the spectrum, but small enough so that the band structure is not ruined and the two ground-bands show “physical” behavior (for example $E(0_2) < E(2_2)$).

The energies of the two ground-bands can be compared with the signatures of the rigid-rotor, spherical-vibrator [12] and $X(5)$ [31]. Table 6.2 lists the intraband energy relations for the different collective terms. It is seen that the two ground-bands arising from the c_3 term are very close to rigid-rotor, the bands arising from the d_3 collective term also seems to resemble the rigid-rotor. This can be explained as the collective operator related with c_3 is composed of a three-body rotational term, $N\hat{C}_{O(3)}$ along with a two-body $N\hat{n}_d$ term. In the large- N limit, the three-body term dominates. A similar explanation can be done for the d_3 term, but here the dominant three-body term is $\hat{n}_d\hat{C}_{O(3)}$.

It can be seen from Table 6.2, that the R values for the first band is decreasing and moves further away from the rigid-rotor region towards the spherical vibrator, as the collective terms are changed from c_3 to c_5 to c_6 . This is also true for the d_i terms, where $i = 3, 5, 6$. The R values for the second band, however, are seem to constantly increase with the d_i coefficients, but not so for the c_i coefficients, where the biggest values are for the c_5 term. For both bands, the R values are smaller for the c_i term, than for its corresponding d_i term. With the exception of the c_5 and d_5 term.

It is interesting to test whether the energies of the two ground-bands, for

	$c_3 = 0.4$	$c_5 = 0.4$	$c_6 = 0.02$
$E(0_2)$	3.641 [3.602]	4.178 [3.390]	0.995 [0.779]
$E(2_2)$	4.613 [4.573]	4.407 [4.313]	1.547 [1.437]
$E(4_1)$	3.333 [3.333]	2.873 [3.250]	2.636 [2.701]
$E(4_2)$	6.880 [6.839]	6.247 [6.532]	3.509 [3.561]
$E(6_1)$	6.999 [6.999]	5.660 [6.758]	5.007 [5.211]
$E(6_2)$	10.445 [10.404]	9.012 [9.981]	6.655 [6.933]
$E(8_1)$	11.998	9.299	8.146
$E(8_2)$	15.311	12.605	10.783

	$d_3 = 0.4$	$d_5 = 0.6$	$d_6 = 0.2$
$E(0_2)$	6.862 [6.832]	7.925 [6.575]	4.820 [3.852]
$E(2_2)$	7.497 [7.472]	8.294 [7.215]	5.055 [4.723]
$E(4_1)$	3.346 [3.352]	3.24 [3.329]	2.967 [3.288]
$E(4_2)$	9.014 [9.006]	9.858 [8.759]	6.876 [6.832]
$E(6_1)$	7.067 [7.099]	6.713 [7.019]	5.944 [6.891]
$E(6_2)$	11.492 [11.523]	12.307 [11.266]	9.702 [10.212]
$E(8_1)$	12.214	11.373	9.89
$E(8_2)$	15.056	15.703	13.526

Table 6.1: The exact [approximated] energies for the critical Hamiltonian with various collective terms. The approximation is discussed at Section 6.1. For each term $E(0_1) = 0$ and $E(2_1) = 1$. Here $h_0 = h_2 = 1$, $\beta_1 = \sqrt{2}$, $\beta_2 = -1$

the different operators, can be interpreted as resulting of a non-rigid body. This is done by comparing the energies of each of the bands with the equation $\alpha L(L+1) + \beta[L(L+1)]^2$, where β is expected to be negative for a non-rigid body. Fitting the different two bands with this equation, the values for α , β and the RMS are given in Table 6.3. It is noted that we cannot always attribute the resulting fit to a non-rigid body, as the β coefficient turns out to be positive for at least one of the bands for all of the collective terms, except c_3 , in which it is almost zero.

The inter- and intra- band transitions of the two ground-bands with the presence of the collective terms are shown in Table 6.4. The intraband transitions are usually stronger than the interband, and the band structure seems to persist in the presence of the collective terms. The c_6 , and to some ex-

	$c_3 = 0.4$	$c_5 = 0.4$	$c_6 = 0.02$	$d_3 = 0.4$	$d_5 = 0.6$	$d_6 = 0.2$
$R_{4_1/2_1}$	3.333	2.873	2.636	3.346	3.24	2.967
$R_{6_1/2_1}$	6.999	5.660	5.007	7.067	6.713	5.944
$R_{8_1/2_1}$	11.998	9.299	8.146	12.214	11.373	9.89
$R_{4_2/2_2}$	3.332	9.035	4.554	3.389	5.238	8.749
$R_{6_2/2_2}$	7.000	21.1092	10.2536	7.29134	11.8753	20.774
$R_{8_2/2_2}$	12.006	36.780	17.732	12.904	21.079	37.047

	rigid-rotor	spherical-vibrator	X(5)
$R_{4/2}$	3.33	2	2.91
$R_{6/2}$	7	3	5.45
$R_{8/2}$	12	4	8.51

Table 6.2: The energy relations for the two bands. Should be compared with the spherical-vibrator, rigid-rotor [12] and X(5) [31], $R_{L_i/2_i} = [E(L_i) - E(0_i)]/[E(2_i) - E(0_i)]$

\tilde{g}_1	$c_3 = 0.4$	$c_5 = 0.4$	$c_6 = 0.02$	$d_3 = 0.4$	$d_5 = 0.6$	$d_6 = 0.2$
α	0.167	0.147	0.135	0.166	0.163	0.151
$\beta(10^{-4})$	0	-2.51	-3.08	0.45	-0.73	-0.19
RMS	0.00007	0.08673	0.13981	0.00043	0.01560	0.06929

\tilde{g}_2	$c_3 = 0.4$	$c_5 = 0.4$	$c_6 = 0.02$	$d_3 = 0.4$	$d_5 = 0.6$	$d_6 = 0.2$
α	0.162	0.102	0.126	0.105	0.094	0.099
$\beta(10^{-4})$	0	2.22	1.47	1.19	2.01	3.08
RMS	0.00208	0.24881	0.14342	0.00042	0.12769	0.23868

Table 6.3: The α, β and the RMS values for the fitting of the equation $\alpha L(L+1) + \beta(L(L+1))^2$ to the ground-bands energies. The energies of $L = 0, 2, 4, 6, 8$ were fitted. Here \tilde{g}_i are the ground-band of the full Hamiltonian.

tent also the d_6 terms, are the only terms that provide substantial interband transitions. Focusing on the c_i terms, and comparing the transitions of the new ground-states. We see that the intraband transitions for the c_3 term, are the closest to those obtained from the intrinsic Hamiltonian, while those that corresponds with c_6 are usually the furthest. The same holds for the d_3 and d_6 terms.

	$c_3 = 0.4$	$c_5 = 0.4$	$c_6 = 0.02$	Intrinsic
$2_2 \rightarrow 0_1$	0.000 [0.000]	0.036 [0.004]	0.061 [0.099]	0.000
$2_2 \rightarrow 0_2$	1.147 [1.126]	0.981 [1.123]	1.002 [1.013]	1.126
$2_2 \rightarrow 2_1$	0.000 [0.000]	0.254 [0.023]	1.296 [1.271]	0.000
$2_2 \rightarrow 4_1$	0.000 [0.000]	0.000 [0.000]	0.287 [0.343]	0.000
$4_1 \rightarrow 2_1$	1.419 [1.420]	1.435 [1.423]	1.258 [1.271]	1.420
$4_2 \rightarrow 2_1$	0.000 [0.000]	0.004 [0.000]	0.208 [0.239]	0.000
$4_2 \rightarrow 2_2$	1.628 [1.600]	1.506 [1.602]	1.355 [1.391]	1.600
$4_2 \rightarrow 4_1$	0.000 [0.000]	0.170 [0.014]	0.291 [0.184]	0.000
$4_2 \rightarrow 6_1$	0.000 [0.000]	0.004 [0.000]	0.031 [0.022]	0.000
$6_1 \rightarrow 4_1$	1.545 [1.548]	1.585 [1.551]	1.514 [1.571]	1.548
$6_2 \rightarrow 4_2$	1.774 [1.746]	1.696 [1.748]	1.688 [1.764]	1.746
$6_2 \rightarrow 6_1$	0.000 [0.000]	0.166 [0.011]	0.066 [0.036]	0.000

	$d_3 = 0.4$	$d_5 = 0.6$	$d_6 = 0.2$	Intrinsic
$2_2 \rightarrow 0_1$	0.000 [0.000]	0.010 [0.000]	0.030 [0.002]	0.000
$2_2 \rightarrow 0_2$	1.154 [1.126]	1.066 [1.125]	0.998 [1.124]	1.126
$2_2 \rightarrow 2_1$	0.000 [0.000]	0.043 [0.003]	0.191 [0.014]	0.000
$2_2 \rightarrow 4_1$	0.000 [0.000]	0.001 [0.000]	0.001 [0.000]	0.000
$4_1 \rightarrow 2_1$	1.422 [1.420]	1.430 [1.420]	1.434 [1.422]	1.420
$4_2 \rightarrow 2_1$	0.000 [0.000]	0.001 [0.000]	0.003 [0.000]	0.000
$4_2 \rightarrow 2_2$	1.639 [1.600]	1.564 [1.600]	1.516 [1.601]	1.600
$4_2 \rightarrow 4_1$	0.000 [0.000]	0.034 [0.002]	0.139 [0.009]	0.000
$4_2 \rightarrow 6_1$	0.000 [0.000]	0.004 [0.000]	0.006 [0.000]	0.000
$6_1 \rightarrow 4_1$	1.552 [1.548]	1.578 [1.548]	1.585 [1.550]	1.548
$6_2 \rightarrow 4_2$	1.788 [1.746]	1.740 [1.746]	1.701 [1.747]	1.746
$6_2 \rightarrow 6_1$	0.000 [0.000]	0.047 [0.003]	0.151 [0.009]	0.000

Table 6.4: $E2$ transitions for the two ground-bands for various collective terms. Here $\chi = 0$ and $2_1 \rightarrow 0_1$ normalized to 1. Approximate results are shown in square brackets, and discussed in Section 6.1. The right column provides the $E2$ transitions for the intrinsic Hamiltonian, where it is understood that the L_i states belong to the g_i band of Section 5.1

6.1 Two-State Mixing

Without the addition of the collective terms, the critical Hamiltonian supports two degenerate ground-bands. For each even- L , there are two (degenerate) states with zero energy that corresponds with the minima of the energy-surface. It is interesting to see if the effect of the addition of the collective terms on the ground-bands can be interpreted as a two-state mixing between the two (formerly) degenerate states (of each L).

It is the purpose of this section to see if the spectrum and transitions presented in the last section can be understood in terms of this mixing. The two state mixing is achieved by degenerate perturbation theory that involves the two degenerate states for each even- L separately. To find the new eigenstates within this approximation, it is enough to calculate the “matrix element” of the Hamiltonian between the two L -projected states of the original ground-bands:

$$\langle \beta_i; N, L | H | \beta_j; N, L \rangle \quad i, j = 1, 2 \quad (6.3)$$

Here $|\beta_i; N, L\rangle, L = 0, 2, 4, \dots$ are the (normalized) ground-band states that are projected from the β_i condensate. When the expression in Eq. (6.3) is found, then the Hamiltonian matrix, restricted to the subspace of the two ground-bands, can be formed and the new eigenstates can be found. We note that by definition, the intrinsic Hamiltonian annihilate the ground-states $H_{int}|\beta_i; N\rangle = 0$. Since H_{int} is an $SO(3)$ scalar, it also annihilates the L -projected states. As a consequence, the calculation of Eq. (6.3) is reduced to the collective terms in the Hamiltonian (H_{col}). The calculation of Eq. (6.3) for each of the collective terms is given in Appendix C.1. The

results, in terms of the parameters of H_{col} in Eq. (6.1) are:

$$\begin{aligned}
m_{12} &\equiv \langle \beta_1; N, L | H | \beta_2; N, L \rangle = \\
&+ c_3(N-2)[L(L+1)S_0^N - 6D_1^N] \\
&+ c_5 \left\{ L(L+1)(D_1^N - 2S_0^N) - 6(D_2^N - D_1^N) \right\} \\
&+ c_6(N-2)(D_2^N - (\beta_1\beta_2)^2 S_2^N) \\
&+ d_3 \left\{ (N-2)(D_2^N - (\beta_1\beta_2)^2 S_2^N) - \left(\frac{\Gamma_N}{\Gamma_{N-1}} \right)^{-1/2} (D_2^{N-1} - (\beta_1\beta_2)^2 S_2^{N-1}) \right\} \\
&+ d_5(N-2)[N(N-1)S_0^N - (1+\beta_1^2)(1+\beta_2^2)S_2^N] \\
&+ d_6 \times 2 \left\{ (N-1)(N-2)[NS_0^N - S_1^N] - (1+\beta_1^2)(1+\beta_2^2)[(N-2)S_2^N - S_3^N] \right\} \\
m_{11} &\equiv \langle \beta_1; N, L | H_{col} | \beta_1; N, L \rangle, \quad m_{22} \equiv \langle \beta_2; N, L | H_{col} | \beta_2; N, L \rangle
\end{aligned} \tag{6.4}$$

where it should be noted that S_n^N , D_n^N and Γ_N depend on β_1 , β_2 and L . They are defined by:

$$\begin{aligned}
\Gamma_N^{(L)}(\beta) &= \frac{1}{N!} \int_0^1 dx [1 + \beta^2 P_2(x)]^N P_L(x) \\
\Gamma_N &\equiv \Gamma_N^{(L)}(\beta_1) \Gamma_N^{(L)}(\beta_2) \\
S_n^N &\equiv \langle \beta_1, L | (s^\dagger)^n (s^\dagger)^n | \beta_2, L \rangle = \frac{\Gamma_{N-n}^{(L)}(\sqrt{\beta_1\beta_2})}{[\Gamma_N^{(L)}(\beta_1) \Gamma_N^{(L)}(\beta_2)]^{1/2}} \\
D_1^N &\equiv \langle \beta_1; N, L | n_d | \beta_2; N, L \rangle = NS_0^N - S_1^N \\
D_2^N &\equiv \langle \beta_1; N, L | (n_d - 1)n_d | \beta_2; N, L \rangle = \\
&\quad (N-1)S_0^N - 2(N-1)S_1^N + S_2^N
\end{aligned} \tag{6.5}$$

with $P_L(x)$ being the Legendre polynomials (with even- L). A slight complications arises from the fact that $|\beta_i; N, L\rangle$ are not orthogonal. This can be

taken into account by transforming into orthogonal basis

$$\begin{aligned}
|\psi_1^{(L)}\rangle &= |\beta_1; N, L\rangle \\
|\psi_2^{(L)}\rangle &= (1 - r_{12}^2)^{-1/2}(|\beta_2; N, L\rangle - r_{12}|\beta_1; N, L\rangle) \\
r_{12} &\equiv \langle \beta_1; N, L | \beta_2; N, L \rangle
\end{aligned} \tag{6.6}$$

and the Hamiltonian 2×2 matrix takes the form

$$\begin{aligned}
K_{11} &= m_{11}, \quad K_{12} = (1 - r_{12}^2)^{-1/2}(m_{12} - r_{12}m_{11}) \\
K_{22} &= (1 - r_{12}^2)^{-1}(m_{22} - 2r_{12}m_{12} + r_{12}^2m_{11})
\end{aligned} \tag{6.7}$$

from which eigenenergies and eigenstates can be found.

To recap, Eq. (6.7) is a matrix representation of the collective Hamiltonian for any L , in the subspace spanned by the two ground-band states $|\beta_1; N, L\rangle$ and $|\beta_2; N, L\rangle$. The eigenvalues and eigenstates of this matrix are the approximated new lowest energies and eigenstates for the full Hamiltonian of Eq. (6.2), containing both the intrinsic and collective terms.

The approximation for the energies is shown in Table 6.1 in square brackets. To test the energies approximation for each of the collective terms, the RMS values for each terms is shown in Table 6.5. It is seen that the best approximation is achieved for the terms that correspond with c_3 and d_3 .

$c_3 = 0.4$	$c_5 = 0.4$	$c_6 = 0.02$	$d_3 = 0.4$	$d_5 = 0.6$	$d_6 = 0.2$
0.032871	0.706836	0.175397	0.0245289	0.946905	0.620367

Table 6.5: The RMS values of the energies for each collective term. Each column specify collective term and the RMS value, calculated by using the exact and approximated energies in Table 6.1

Each exact state $|L_i\rangle$ of the critical Hamiltonian can be written as a combination of the two L -projected states, $|\beta_i; N, L\rangle$, $i = 1, 2$, and another state, orthogonal to both. That is $|L_i\rangle = \alpha_1|\beta_1; N, L\rangle + \alpha_2|\beta_2; N, L\rangle + \gamma|O; N, L\rangle$, where $\langle O; N, L | \beta_i; N, L \rangle = 0$. The parameter γ^2 shows to what extent the two-state approximation is valid. The ratio between α_1 and α_2 quantify the mixing. Table 6.6 gives the exact [approximated] values for some of the

	$c_3 = 0.4$			$c_5 = 0.4$			$c_6 = 0.02$		
	α_1^2	α_2^2	γ^2	α_1^2	α_2^2	γ^2	α_1^2	α_2^2	γ^2
0_1	0.992 [1.0]	0.000 [0.0]	0.008	0.793 [0.985]	0.097 [0.014]	0.108	0.465 [0.438]	0.528 [0.557]	0.003
0_2	0.000 [0.0]	0.998 [1.0]	0.002	0.132 [0.015]	0.833 [0.986]	0.038	0.534 [0.562]	0.470 [0.443]	0.001
2_1	0.992 [1.0]	0.000 [0.0]	0.008	0.862 [0.996]	0.036 [0.004]	0.102	0.675 [0.708]	0.320 [0.289]	0.002
2_2	0.000 [0.0]	0.998 [1.0]	0.002	0.046 [0.004]	0.867 [0.996]	0.087	0.323 [0.292]	0.678 [0.711]	0.001

	$d_3 = 0.4$			$d_5 = 0.6$			$d_6 = 0.2$		
	α_1^2	α_2^2	γ^2	α_1^2	α_2^2	γ^2	α_1^2	α_2^2	γ^2
0_1	0.986 [1.0]	0.000 [0.0]	0.014	0.914 [0.998]	0.015 [0.001]	0.070	0.824 [0.991]	0.072 [0.008]	0.10
0_2	0.000 [0.0]	0.998 [1.0]	0.002	0.026 [0.002]	0.936 [0.999]	0.039	0.102 [0.009]	0.861 [0.992]	0.04
2_1	0.987 [1.0]	0.000 [0.0]	0.013	0.925 [0.999]	0.005 [0.000]	0.070	0.877 [0.997]	0.026 [0.002]	0.09
2_2	0.000 [0.0]	0.998 [1.0]	0.002	0.008 [0.001]	0.927 [1.000]	0.065	0.035 [0.003]	0.880 [0.998]	0.086

Table 6.6: The exact [approximated] decomposition of the two ground-bands into the non-perturbed ground-band states in the presence of the collective terms. Each eigenstate is written as $|L_i\rangle = \alpha_1|\beta_1; N, L\rangle + \alpha_2|\beta_2; N, L\rangle + \gamma|O\rangle$, where $\langle\beta_i; N, L|O\rangle = 0$. Note that in general $\alpha_1^2 + \alpha_2^2 + \gamma^2 \neq 1$

states, decomposed into the states mentioned above.

It can be seen that the mixing is small for most of the collective terms, and at least for the values of the coefficients selected, the probability of the states to be outside of the subspace spanned by the two states is also small (for most cases $\approx 1\%$). The mixing is strong for the $L = 0, 2$ eigenstates of the $\hat{N}\hat{C}_{\overline{O(6)}}$ term. These results can explain the exact energies obtained by numerical procedure. The fact that γ^2 is small for most terms show that the two-state approximation is valid, and that energies can be obtained by this approximation. The collective terms seem to split the energies, but they do not contribute to the mixing between the two states.

The two state mixing can also be used to calculate the approximate $E2$ intra- and inter- transitions. This is done by writing each of the states $|L_i\rangle$ as $|L_i\rangle = \alpha_1^{L_i}|\beta_1; N, L\rangle + \alpha_2^{L_i}|\beta_2; N, L\rangle$, where the α_i are the coefficients found using the two-state mixing. With this, the transition probability is (see Section 1.4):

$$B(E2; L_i \rightarrow L'_j) = \left| \sum_{m,n} \alpha_n^{L_i} (\alpha_m^{L'_j})^* (\langle\beta_m; L', N||T^{(2)}||\beta_n; L, N\rangle (2L+1)^{-1/2}) \right|^2 \quad (6.8)$$

where the terms in the parenthesis are given in Eq. (C.2.11) ($e_b = 1$, see Appendix C.2 for a detailed calculation).

The exact [approximated] results for the $E2$ transitions and for the various collective terms are given in Table 6.4. It can be seen that for some of the cases, the approximated results do not differ much from the results of the intrinsic Hamiltonian. This again is a consequence of the fact that most of the collective terms seem not to mix between the degenerate ground-band states, and mostly contribute to the energy splitting. The $L = 0, 2$ states of the $\hat{N}\hat{C}_{\overline{O(6)}}$ terms are unique in that sense, as they produce a large mixing between the states. As a consequence there is a big difference between the transitions of the intrinsic Hamiltonian and complete Hamiltonian for these states.

Chapter 7

Conclusions and Outlook

Phase transitions in nuclei are a widely discussed topic. In particular the coexistence of different phases, as observed in many nuclei, is an interesting and active topic of research. The two-body IBM Hamiltonian was used to model many nuclei, but it is not able describe a coexistence between two deformed minima.

In this work we have set the first steps towards understanding first-order phase transitions and coexistence of axially-deformed shapes in nuclei, using the three-body IBM. The main result of this work was to identify the relevant interactions and build the critical Hamiltonian for a degenerate deformed-deformed coexistence with three-body terms.

We have used the intrinsic and collective resolution in-order to find the relevant interactions. The condition $R|\beta_i, 0; N\rangle = 0$ was used on two different condensates, which allowed us to identify the three-body intrinsic operators relevant for the deformed-deformed coexistence. With these conditions, we found that the intrinsic part of the critical Hamiltonian can be written using two three-body operators:

$$H = h_0 R_0^\dagger \tilde{R}_0 + h_2 R_2^\dagger \cdot \tilde{R}_2$$

with $h_0, h_2 \geq 0$, where R_0 is the a three-boson operator with angular momentum $L = 0$, and the R_2 operator has angular momentum of $L = 2$. An

interesting consequence of these results was the ability to combine two different PDS in the same Hamiltonian, namely, Hamiltonian in which part of the states have an $SO(6)$ symmetry, while part of the states have an $SU(3)$ symmetry and all the other states are mixed.

The energy-surface of the two operators was thoroughly analyzed (Chapter 4). We found that the $R_0^\dagger \tilde{R}_0$ operator has a 'trajectory' in the (β, γ) plane for which its energy is zero. This also reflects in the fact that this operator annihilates a continuity of condensates, $|\beta, \gamma = f(\beta); N\rangle$. The $R_2^\dagger \cdot \tilde{R}_2$ operator was found to have only additional other minimum, at $\beta = 0$, and the inclusion of the two terms in the same Hamiltonian was found to give rise to an energy surface with two minima only: $(\beta_i, \gamma = 0)$ or $(|\beta_i|, \gamma = \pi/3)$ if $\beta_i < 0$, with $i = 1, 2$.

As a result of the energy-surface analysis, and because $R_0^\dagger \tilde{R}_0$ have more than the required two condensate eigenstates, we have concluded that this operator cannot describe a critical Hamiltonian by itself. We must require $h_2 > 0$. The second operator, $R_2^\dagger \cdot \tilde{R}_2$ however, was found to support a shape coexistence of three shapes: two deformed and spherical. This is the only intrinsic operator in the IBM (at least up to three-body interactions) that can be used to describe such coexistence. As such, this operator is of potential relevance for heavy nuclei that show coexistence of three shapes (for example ^{186}Pb [6]).

The analysis of the particular energy-surface with $h_0 = h_2$ showed that when the two operators were combined, then the energy-barrier of the critical Hamiltonian was usually much higher for the prolate-oblate case than the prolate-prolate (or oblate-oblate) cases. These points should be further studied for different critical Hamiltonians, as the typical shape coexistence in nuclei is found to be a prolate-oblate one.

The spectrum and transition of the critical Hamiltonian were also considered. Except for the two degenerate ground-bands, which are part of the critical Hamiltonian construction, we were able to identify the two β - and two γ - bands using an analysis of the spectrum and transitions-strength. A

comparison with the Alaga rules further confirmed that the ground- and β -bands are indeed bands with $K = 0$, and that the γ_1 , γ_2 and $\gamma_1\beta_1$ bands are bands with $K = 2$ (see Figures 5.2, 5.3).

In addition to the spectrum analysis, we have approximated the critical Hamiltonian via normal modes around each minima. This approach was used to identify the excited bands with their corresponding minima, and a wave-function analysis confirmed this identification. The expansion into normal-modes also gave us some insight about the bandhead energies of the different bands. It was shown that the ratio between the two γ -bands is independent of the coefficients h_0, h_2 , and is only affected by the choice of β_1, β_2 . Furthermore, for a spherical-deformed-deformed situations ($h_0 = 0$), it was shown that once the ratios between the two β -bands bandhead energies, and the two γ -band bandhead energies are fixed, then β_1^2, β_2^2 are set.

Lastly, we explored the effect of adding collective terms to the intrinsic Hamiltonian. The different terms were added separately and their effect on the spectrum and transitions of the two (formerly degenerate) ground-bands were considered. Even with the addition of the collective terms, the energies and transitions showed that the band-structure persists. The two ground-bands energies and transitions were approximated by using a two-state mixing approach. This showed a good agreement with the energies and transitions for most cases, and it was shown that the effect of most of the collective terms was to split the degeneracy between the two bands, but it did not tend to mix them. An exception to this behavior appeared with the collective term that is related with $\hat{N}\hat{C}_{O(6)}$, this term was shown to strongly mix the two bands $L = 0, 2$ states.

At this point there are a few important topics that can be studied. The first is to extend the study of the three-body Hamiltonian away from the critical point. This work has focused on the critical Hamiltonian, but there is a need to study the full evolution of the QPT. A second goal is to examine candidate nuclei, based on the derived signatures. Another interesting problem that remains open is to find the constraints on the most-general three-body

energy surface, such that the surface supports two degenerate minima. This approach can be used to employ the full Hamiltonian directly.

Bibliography

- [1] M. Vojta, *Quantum phase transitions*, Reports on Progress in Physics **66**, 2069 (2003).
- [2] M. Greiner, O. Mandel, T. Esslinger, T. W. Hänsch, and I. Bloch, *Quantum phase transition from a superfluid to a mott insulator in a gas of ultracold atoms*, Nature **415**, 39–44 (2002).
- [3] P. Cejnar, J. Jolie, and R. F. Casten, *Quantum phase transitions in the shapes of atomic nuclei*, Reviews of Modern Physics **82**, 2155 (2010).
- [4] E. Clément, A. Görgen, W. Korten, E. Bouchez, A. Chatillon, J.-P. Delaroche, M. Girod, H. Goutte, A. Hürstel, Y. Le Coz, et al., *Shape coexistence in neutron-deficient krypton isotopes*, Physical Review C **75**, 054313 (2007).
- [5] H. Iwasaki, A. Lemasson, C. Morse, A. Dewald, T. Braunroth, V. Bader, T. Baugher, D. Bazin, J. Berryman, C. Campbell, et al., *Evolution of collectivity in ^{72}Kr : evidence for rapid shape transition*, Physical Review Letters **112**, 142502 (2014).
- [6] A. Andreyev, M. Huyse, P. Van Duppen, L. Weissman, D. Ackermann, J. Gerl, F. Hessberger, S. Hofmann, A. Kleinböhl, G. Münzenberg, et al., *A triplet of differently shaped spin-zero states in the atomic nucleus ^{186}Pb* , Nature **405**, 430–433 (2000).
- [7] M. Kimura, Y. Taniguchi, Y. Kanada-En'yo, H. Horiuchi, and K. Ikeda, *Prolate, oblate, and triaxial shape coexistence, and the lost magicity of $N = 28$ in ^{43}S* , Physical Review C **87**, 011301 (2013).

- [8] A. Arima and F. Iachello, *Collective nuclear states as representations of a $SU(6)$ group*, Physical Review Letters **35**, 1069 (1975).
- [9] J. Jolie, P. Cejnar, R. Casten, S. Heinze, A. Linnemann, and V. Werner, *Triple point of nuclear deformations*, Physical Review Letters **89**, 182502 (2002).
- [10] F. Iachello and N. Zamfir, *Quantum phase transitions in mesoscopic systems*, Physical Review Letters **92**, 212501 (2004).
- [11] A. Leviatan and B. Shao, *General quadrupole nuclear shapes. An algebraic perspective*, Physics Letters B **243**, 313–318 (1990).
- [12] R. Casten and D. Warner, *The interacting boson approximation*, Reviews of Modern Physics **60**, 389 (1988).
- [13] F. Iachello and A. Arima, *The interacting boson model* (Cambridge University Press, 1987).
- [14] J. Elliott, *Collective motion in the nuclear shell model. I. Classification schemes for states of mixed configurations*, Proceedings of the Royal Society of London. Series A. Mathematical and Physical Sciences **245**, 128–145 (1958).
- [15] A. Bohr and B. R. Mottelson, *Nuclear structure*, Vol. 1 (World Scientific, 1998).
- [16] J. Ginocchio and M. Kirson, *An intrinsic state for the interacting boson model and its relationship to the Bohr-Mottelson model*, Nuclear Physics A **350**, 31–60 (1980).
- [17] A. Arima and F. Iachello, *Interacting boson model of collective states I. The vibrational limit*, Annals of Physics **99**, 253–317 (1976).
- [18] A. Arima and F. Iachello, *Interacting boson model of collective nuclear states II. The rotational limit*, Annals of Physics **111**, 201–238 (1978).
- [19] A. Arima and F. Iachello, *Interacting boson model of collective nuclear states IV. The $O(6)$ limit*, Annals of Physics **123**, 468–492 (1979).

- [20] A. Leviatan, *Non-spherical boson basis for near- $O(6)$ nuclei*, Physics Letters B **143**, 25–30 (1984).
- [21] H. T. Chen and A. Arima, *Cylindrical $\bar{s}p$ -boson model for large deformed nuclei*, Physical Review Letters **51**, 447 (1983).
- [22] A. Leviatan, *Intrinsic and collective structure in the interacting boson model*, Annals of Physics **179**, 201–271 (1987).
- [23] M. W. Kirson and A. Leviatan, *Resolution of any interacting-boson-model hamiltonian into intrinsic and collective parts*, Physical Review Letters **55**, 2846 (1985).
- [24] A. Leviatan, *Partial dynamical symmetries*, Progress in Particle and Nuclear Physics **66**, 93–143 (2011).
- [25] A. Leviatan, *Partial dynamical symmetry in deformed nuclei*, Physical Review Letters **77**, 818 (1996).
- [26] R. Casten, R. Cakirli, K. Blaum, and A. Couture, *Evidence for partial dynamical symmetries in atomic nuclei*, Physical Review Letters **113**, 112501 (2014).
- [27] A. Couture, R. Casten, and R. Cakirli, *Extended tests of an $SU(3)$ partial dynamical symmetry*, Physical Review C **91**, 014312 (2015).
- [28] A. Leviatan and P. Van Isacker, *Generalized partial dynamical symmetry in nuclei*, Physical Review Letters **89**, 222501 (2002).
- [29] C. Kremer, J. Beller, A. Leviatan, N. Pietralla, G. Rainovski, R. Trippe, and P. Van Isacker, *Linking partial and quasi dynamical symmetries in rotational nuclei*, Phys. Rev. C **89**, 041302 (2014).
- [30] A. Dieperink, O. Scholten, and F. Iachello, *Classical limit of the interacting-boson model*, Physical Review Letters **44**, 1747 (1980).
- [31] F. Iachello, *Analytic description of critical point nuclei in a spherical-axially deformed shape phase transition*, Physical Review Letters **87**, 052502 (2001).

- [32] A. Leviatan, *X(5) critical-point structure in a finite system*, Physical Review C **72**, 031305 (2005).

Appendix A

Critical Hamiltonian Energy Surface

This section contains the analysis of the two energy surfaces. For completeness, the hessian along the $\gamma = 0$ line, for the general three-body energy surface is given:

$$\begin{aligned}\left.\frac{\partial^2 E}{\partial \beta^2}\right|_{\gamma=0} &= 2\frac{\beta^7 C + 3\beta^6(D - 3(A + B))}{(1 + \beta^2)^5} \\ &+ 2\frac{\beta^5(6E - 13C) + 5\beta^4(3(A + B - D) + 2F)}{(1 + \beta^2)^5} \\ &+ 2\frac{+5\beta^3(2C - 3E) + \beta^2(6D - 13F) + 3\beta E + F}{(1 + \beta^2)^5} \quad (\text{A.0.1}) \\ \left.\frac{\partial^2 E}{\partial \gamma^2}\right|_{\gamma=0} &= \frac{9\beta^3(\beta^2(2\beta B + C) + E)}{(1 + \beta^2)^3} \\ \left.\frac{\partial^2 E}{\partial \beta \partial \gamma}\right|_{\gamma=0} &= 0\end{aligned}$$

A.1 $R_0^\dagger R_0$ Energy Surface

This section gives a derivation of the important features of the $R_0^\dagger R_0$ energy surface. First we identify that this energy surface has a trajectory in the (β, γ) plane with zero energy, and find this trajectory. then the other extrema

points are identified. Lastly we find the energy barrier between the global minima.

Inspecting the energy surface equation (4.4), and defining $\Gamma = \cos(3\gamma)$ we solve for $\Gamma = f(\beta)$ such that $E_0(\beta, \gamma) = 0$. For $0 \leq \gamma \leq \pi/3$ we must require

$$\cos(3\gamma) \equiv \Gamma = \frac{\beta^2(\beta_1^2 + \beta_1\beta_2 + \beta_2^2) - \beta_1^2\beta_2^2}{(\beta_1 + \beta_2)\beta^3}, \quad |\Gamma| < 1 \quad (\text{A.1.1})$$

Since $\Gamma(\beta)$ is a continuous function of β , it is enough to test Γ at the boundaries $\Gamma = -1, 1$ to understand for which values of β we have a solution. The values of β for which $\Gamma = \pm 1$ are known from the energy-surface equation with $\gamma = 0$ (4.6). These are $\beta = \beta_1, \beta_2$ for $\Gamma = 1$, and $\beta = -\beta_3$ for $\Gamma = -1$ (the minus sign is due to the fact that here β is treated as a radius variable and we use $\gamma = \pi/3$). Differentiating Eq. (A.1.1) with respect to β and plugging the roots, we obtain

$$\begin{aligned} \frac{d\Gamma}{d\beta}\Big|_{\beta=-\beta_3} &= \frac{(\beta_1 + \beta_2)(2\beta_1 + \beta_2)(2\beta_2 + \beta_1)}{\beta_1^2\beta_2^2} \\ \frac{d\Gamma}{d\beta}\Big|_{\beta=\beta_2} &= \frac{(\beta_1 - \beta_2)(2\beta_1 + \beta_2)}{\beta_2^2(\beta_1 + \beta_2)} \end{aligned} \quad (\text{A.1.2})$$

We see that at $\beta = -\beta_3$ the derivative is always positive, while for the two other roots it is positive only for the smaller root and negative for the bigger one.

The last two equations are to be interpreted as follows: there are two non-connected trajectories in the (β, γ) plane for which $E_0(\beta, \gamma) = 0$. Choosing $0 < \beta_2 < \beta_1$, there is one trajectory that begins at $(\beta_1, 0)$ and continues with a growing β towards the $(\infty, \pi/6)$ point. The other trajectory connects between the $(-\beta_3, \pi/3)$ and the $(\beta_2, 0)$ points (see Fig. 4.1, p. 25).

The next step in analyzing the energy surface is to find the other extrema points for the surface. Differentiating Eq. (4.4) with respect to γ it is seen immediately that the extrema points must lie either on the trajectories already discussed, or on the $\gamma = 0, \pi/3$ line. Setting $\gamma = 0$, the solutions for the other extrema is found by solving $\partial E_0(\beta, 0)/\partial\beta = 0$, where the $\beta < 0$

solutions are identified with $\gamma = \pi/3, \beta \rightarrow |\beta|$. Differentiating with respect to β we find

$$\begin{aligned} \partial E_0(\beta, 0)/\partial\beta = 0 &\Rightarrow \\ \beta(\beta - \beta_1)(\beta - \beta_2)(\beta - \beta_3)F(\beta, \beta_1, \beta_2) &= 0 \end{aligned} \quad (\text{A.1.3})$$

with

$$\begin{aligned} F(\beta; \beta_1, \beta_2) &= \beta^2 (\beta_1^2 + \beta_1\beta_2 + \beta_2^2) + 3\beta(\beta_1 + \beta_2) - 2(\beta_1\beta_2 + \beta_2^2 + \beta_1^2) \\ A(\beta) &> 0 \end{aligned} \quad (\text{A.1.4})$$

Eliminating the three known minima solutions $(\beta_1, \beta_2, \beta_3)$, we find the three extrema

$$\begin{aligned} \beta_0 = 0, \quad \beta_F^{+/-} &= \frac{-3(\beta_1 + \beta_2) \pm \Delta}{2(\beta_1^2 + \beta_1\beta_2 + \beta_2^2)} \\ \Delta &= \sqrt{9(\beta_1 + \beta_2)^2 + 4(\beta_1^2 + \beta_1\beta_2 + \beta_2^2)(2(\beta_1^2 + \beta_1\beta_2 + \beta_2^2) + 3\beta_1^2\beta_2^2)} \end{aligned} \quad (\text{A.1.5})$$

Fixing $\gamma = 0$ and considering the energy surface as a function of β only $\tilde{E}(\beta) = E_0(\beta, 0)$, the solution $\beta = \beta_F^+$ is positive, and so it must satisfy $\beta_2 < \beta_F^+ < \beta_1$ and be a maximum of $\tilde{E}(\beta)$. The $\beta = 0$ extremum is a maximum as well. The last extremum $\beta = \beta_F^-$ fulfill $\beta_F^- < \beta_3$ and is also a maximum of $\tilde{E}(\beta)$. This is since it is evident from Eq. (A.1.5) that $\beta_3 < 0$, in addition it cannot be an inflection point because this requires that the derivative of the energy surface with respect to β in Eq. (A.1.3) will be proportional to $(\beta - \beta_3)^{2n}$, with n integer. As a consequence it cannot be positioned between β_3 and β_0 .

To test whether the points $(\beta_0, 0), (\beta_F^+, 0), (\beta_F^-, 0)$ are real maxima, the Hessian should be calculated. It is already diagonal for $\gamma = 0$ [11], accordingly it is enough to calculate $d^2 E_0/d\gamma^2$. The result is

$$\frac{\partial^2 E_0}{\partial\gamma^2} \Big|_{\gamma=0} = \frac{-36\beta^3(\beta - \beta_1)(\beta - \beta_2)(\beta - \beta_3)}{35(1 + \beta^2)^3} \quad (\text{A.1.6})$$

which shows that β_F^+ is a saddle and β_F^- is a maximum (see Fig. 4.1).

That the second derivative of the energy surface with respect to γ is zero for $\beta = \beta_i$ ($i = 1, 2, 3$) is a consequence of the zero-energy trajectories described above.

The last result which is of interest for the current section is the energy barrier between the global minima. From the analysis of the global minima we see that such barrier does not exist between the points $(\beta_2, 0)$ and $(\beta_3, 0)$. To find the barrier between the two minima $(\beta_1, 0)$ and $(\beta_2, 0)$, we note that the function $E_0(\beta, \gamma)$ where $\beta \in (\beta_2, \beta_1)$ is monotonically increasing in γ . Furthermore, any trajectory between the two minima must cross the arc $(\beta, \gamma(t)), t \in [0, \pi/3]$ where β is fixed such that $\beta_2 < \beta < \beta_1$. Using this fact it is clear that the energy barrier is located at $(\beta_F^+, 0)$, which is the highest point on the line $\gamma = 0$ that connects the two points.

A.2 $R_2^\dagger \cdot \tilde{R}_2$ Energy Surface

This section derives the properties of the extrema points and the location of the energy barrier. The energy surface is monotonic in γ , and the condition for the extrema points read

$$\left. \frac{\partial E_2(\beta, \gamma)}{\partial \beta} \right|_{\gamma=0} = 0$$

$$\frac{\beta(\beta - \beta_1)(\beta - \beta_2) \left(\beta^3(\beta_1 + \beta_2) + \beta^2(3 - 2\beta_1\beta_2) - 2\beta(\beta_1 + \beta_2) + \beta_1\beta_2 \right)}{(1 + \beta^2)(\beta_1 + \beta_2)} = 0 \quad (\text{A.2.1})$$

The three unknown extrema are the solutions of the equation

$$\beta^3(\beta_1 + \beta_2) + \beta^2(3 - 2\beta_1\beta_2) - 2\beta(\beta_1 + \beta_2) + \beta_1\beta_2 = 0 \quad (\text{A.2.2})$$

There are three global minima $0, \beta_2, \beta_1$, and as such at least two maxima must be positioned between them. Denoting the two maxima β_1^m, β_2^m , this leaves the third extrema β_3^m unknown. It will now be shown that β_3^m is a

maximum.

First, β_3^m cannot be an inflection point. This requires a Eq. (A.2.2) to be proportional to $(\beta - \beta_3^m)^2$. In addition, it cannot be a minimum, because then there would have been two minima without a maximum between them.

It follows that β_3^m is a maximum. It must be that $\beta_3^m > \max(\beta_1, \beta_2, 0)$ or $\beta_3^m < \min(\beta_1, \beta_2, 0)$ (otherwise there would be two adjacent maxima without a minimum between them). The sign of β_3^m can be found from the equation

$$-\beta_1^m \beta_2^m \beta_3^m = \frac{\beta_1 \beta_2}{\beta_1 + \beta_2} \quad (\text{A.2.3})$$

For $0 < \beta_2 < \beta_1$ then $\beta_3^m < 0$. For $\beta_2 < 0 < \beta_1$ then the sign of β_3^m depends on the expression $\beta_1 + \beta_2$: If $\beta_1 + \beta_2 > 0$, then $\beta_3^m < 0$, while for $\beta_1 + \beta_2 < 0$ we have $\beta_3^m > 0$ (this is also evident from the symmetry discussed in Section 4.2).

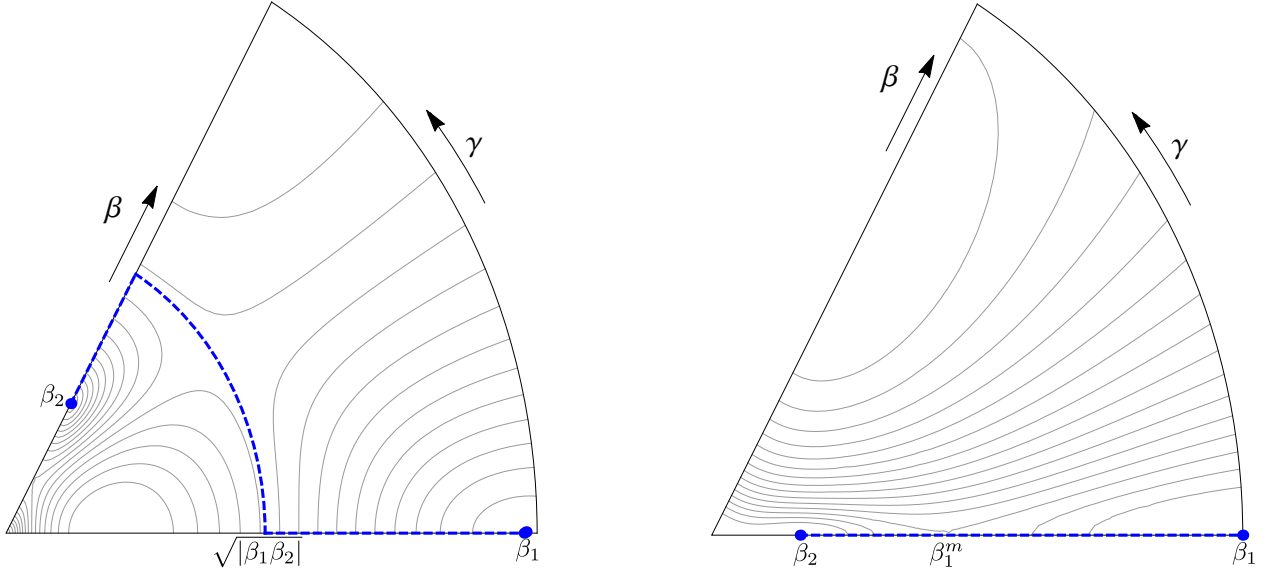
The next section will deal with the energy barrier. The energy surface is

$$E_2(\beta, \gamma; \beta_1, \beta_2) = N(N-1)(N-2) \times \frac{2\beta^2 \{ \beta^4 - 2(\beta_1 + \beta_2)(\beta^2 + \beta_1\beta_2)\beta \cos 3\gamma + (\beta_1^2 + 4\beta_2\beta_1 + \beta_2^2)\beta^2 + \beta_1^2\beta_2^2 \}}{7(1 + \beta^2)^3 (\beta_1 + \beta_2)^2} \quad (\text{A.2.4})$$

We see that for a fixed β , the energy surface is a monotonic function of γ , either increasing or decreasing.

For the case $0 < \beta_2 < \beta_1$ (where the two minima are positioned along the $\gamma = 0$ line), the energy surface is always increasing in the positive γ direction, and so the energy barrier must lie on the $\gamma = 0$ line. It is located in the $(\beta_1^m, 0)$ point. This expression can be calculated, but its analytic form is complicated.

For the second case, where $\beta_2 < 0 < \beta_1$ and $\beta_1 > |\beta_2|$, the energy decreases in the positive γ direction for $\beta \in [-\beta_2, \sqrt{|\beta_1\beta_2|})$ and increases in the positive γ direction for $\beta \in (\sqrt{|\beta_1\beta_2|}, \beta_1]$. Consequently, if the system moves between the two minima along the line that connects between $(-\beta_2, \pi/3)$ and



(a) Negative and positive minima. The energy barrier is $E_2(\sqrt{|\beta_1\beta_2|})$, and is located on the arc $\beta = \sqrt{|\beta_1\beta_2|}$, $\gamma =$ arbitrary

(b) Two positive minima. The energy barrier is located at $(\beta = \beta_1^m, \gamma = 0)$, and β_1^m is the biggest solution of Eq. (A.2.2)

Figure A.2.1: $R_2^\dagger \cdot \tilde{R}_2$ energy-surface. The dashed line shows the trajectory that passes between the two minima and through the energy barrier.

$(\sqrt{|\beta_1\beta_2|}, \pi/3)$, the arc $(\sqrt{|\beta_1\beta_2|}, \gamma), \gamma \in [0, \pi/3]$ and the line that connects between the points $(\beta_1, 0)$ and $(\sqrt{|\beta_1\beta_2|}, 0)$, see Fig. A.2.1. then the highest point along this trajectory will be the energy barrier. This point is found, as explained above, on the $\beta = \sqrt{|\beta_1\beta_2|}$ arc. The energy at this point is

$$E_{\text{barrier}} = E(\sqrt{|\beta_1\beta_2|}, \gamma; \beta_1, \beta_2) = N(N-1)(N-2) \frac{2(\beta_1\beta_2)^2}{7(1+|\beta_1\beta_2|)^3} \quad (\text{A.2.5})$$

Appendix B

$O(6)$ - $\langle\sigma\rangle$ Decomposition of the Intrinsic States

The normal-mode expansion allows to define the β - and γ - bands around each minima by $SO(3)$ projection from the intrinsic states defined in Eq. (1.7). This section aims to show the decomposition of the β and γ intrinsic states for $\beta = -1, \gamma = 0$ into the $SO(6)$ σ -components

The intrinsic β -state and its σ -decomposition is given by:

$$|b_\beta; N\rangle \equiv \frac{1}{\sqrt{(N-1)!}} b_\beta^\dagger (b_c^\dagger)^{N-1} |0\rangle = \sqrt{\frac{N-1}{N+1}} |\sigma = N-2\rangle + \sqrt{\frac{2}{N+1}} |\sigma = N\rangle \quad (\text{B.0.1})$$

Here $b_c^\dagger, b_\beta^\dagger$ are the usual GNSB operators with $\beta = -1$ and $\gamma = 0$ (see Section 1.2.2).

The method by which Equation (B.0.1) is proved, is by applying the Casimir $P_0^\dagger P_0 = [-\hat{C}_{O(6)} + N(N+4)]$, where $P_0^\dagger = d^\dagger \cdot d^\dagger - (s^\dagger)^2$, to the state $|b_\beta; N\rangle$. First, it is clear that this state can contain only irreps of $\langle N \rangle$ and $\langle N-2 \rangle$, since $(b_c^\dagger)^{(N-1)}$ has a good $\langle \sigma = N-1 \rangle$ label, and b_β has a good $\langle \sigma = 1 \rangle$ label. Thus it can be written as $|b_\beta; N\rangle = a_0 |\sigma = N\rangle + a_2 |\sigma = N-2\rangle$. Applying $P_0^\dagger P_0$ to this vector, the vector that belongs to the $\langle \sigma = N \rangle$ is

nullified, and we are left with the second vector:

$$P_0^\dagger P_0 |b_\beta; N\rangle = [-\sigma(\sigma + 4) + N(N + 4)]a_2 |\sigma = N - 2\rangle = 4(1 + N)a_2 |\sigma = N - 2\rangle$$

The norm of this expression is

$$\| |b_\beta; N\rangle \|^2 = 16(1 + N)^2 a_2^2 \quad (\text{B.0.2})$$

On the other hand, this result can be calculated directly with the help of the commutation relations. First we note that $(b_c^\dagger = s^\dagger - d_0^\dagger, b_\beta^\dagger = s^\dagger + d_0^\dagger)$:

$$P_0^\dagger = d^\dagger \cdot d^\dagger - (s^\dagger)^2 = 2[-b_c^\dagger b_\beta^\dagger + d_2^\dagger d_{-2}^\dagger - d_1^\dagger d_{-1}^\dagger] \quad (\text{B.0.3})$$

and applying the Casimir we have

$$\begin{aligned} P_0^\dagger P_0 \frac{1}{\sqrt{(N-1)!}} b_\beta^\dagger (b_c^\dagger)^{N-1} |0\rangle &= \\ P_0^\dagger [-2b_\beta b_c] \frac{1}{\sqrt{(N-1)!}} b_\beta^\dagger (b_c^\dagger)^{N-1} |0\rangle &= \\ -2P_0^\dagger \frac{\sqrt{N-1}}{\sqrt{(N-2)!}} (b_c^\dagger)^{N-2} |0\rangle &= \\ -4[-b_c^\dagger b_\beta^\dagger + d_2^\dagger d_{-2}^\dagger - d_1^\dagger d_{-1}^\dagger] \frac{\sqrt{N-1}}{\sqrt{(N-2)!}} (b_c^\dagger)^{N-2} |0\rangle & \end{aligned} \quad (\text{B.0.4})$$

Taking the norm of (B.0.4), we use the commutation relations $[d_\mu, d_\mu^\dagger] = 1$ and the fact that the bosons $b_\beta, b_c, d_\mu (\mu = -2, -1, 1, 2)$ are orthogonal and that $d_\mu^\dagger d_\mu$ functions as number operators (as well as $b_c^\dagger b_c$ and $b_\beta^\dagger b_\beta$). We then have:

$$\begin{aligned} \| P_0^\dagger P_0 \frac{1}{\sqrt{(N-1)!}} b_\beta^\dagger (b_c^\dagger)^{N-1} |0\rangle \|^2 &= \\ 16\{(1 + (N-2)) \cdot 1 + 1 + 1\}(N-1) &= 16(N-1)(N+1) \end{aligned} \quad (\text{B.0.5})$$

Comparing (B.0.2) with (B.0.5), we find $a_2 = \sqrt{\frac{N-1}{N+1}}$. a_0 is then found to

$$\text{be } a_0 = \sqrt{1 - a_2^2} = \sqrt{\frac{2}{N+1}}$$

The intrinsic γ -state that corresponds with the condensate $|-1, 0; N\rangle$ is orthogonal to the β -band. As such it can be written as (see Eq. B.0.1):

$$\begin{aligned} |b_\gamma; N\rangle &\equiv \frac{1}{\sqrt{(N-1)!}} b_\gamma^\dagger (b_c^\dagger)^{N-1} |0\rangle \\ &= \alpha \left(\sqrt{\frac{2}{N+1}} |\sigma = N-2\rangle - \sqrt{\frac{N-1}{N+1}} |\sigma = N\rangle \right) + |\nu\rangle \end{aligned} \quad (\text{B.0.6})$$

where $|\nu\rangle$ is orthogonal to the two other states. In addition, the d_μ^\dagger have a good $\langle \sigma = 1 \rangle$ label. It follows that $|\nu\rangle = 0$ and

$$|b_\gamma; N\rangle = \sqrt{\frac{2}{N+1}} |\sigma = N-2\rangle - \sqrt{\frac{N-1}{N+1}} |\sigma = N\rangle \quad (\text{B.0.7})$$

Appendix C

Matrix Elements of the Collective Hamiltonian

C.1 Calculation of the Collective Matrix Terms

This section contains the “sandwiching” of the operators that compose the collective Hamiltonian between the L -projected intrinsic states. Using these calculations, the m_{ij} matrix $m_{ij} = \langle \beta_i; N, L | H_{col} | \beta_j; N, L \rangle$ of Chapter 6 can be evaluated.

In the $U(5)$ basis, the condensate states can be written as [32]:

$$|\beta; N, L\rangle = \sum_{\tau \leq n_d \leq N, \tau, n_\Delta} \frac{1}{2} [1 + (-1)^{n_d - \tau}] \xi_{n_d, \tau, n_\Delta}^{(N, L)} |N, n_d, \tau, n_\Delta, L\rangle \quad (\text{C.1.1})$$

and

$$\xi_{n_d, \tau, n_\Delta}^{(N, L)} = [\Gamma_N^{(L)}(\beta)]^{-1/2} f_{\tau, n_\Delta}^{(L)} \frac{\beta^{n_d}}{[(N - n_d)!(n_d - \tau)!(n_d + \tau + 3)!]^{1/2}}$$

where $\Gamma_N^{(L)}(\beta)$ is the normalization factor: $[\Gamma_N^{(L)}(\beta)] \propto \|P_L|N, \beta\rangle\|^2$. First the expression $\langle \beta_i; N, L | (s^\dagger)^n s^n | \beta_j; N, L \rangle$ will be calculated, then the other terms will be calculated using it.

Calculating $s|\beta; N, L\rangle$

We note that:

$$\begin{aligned} \xi_{n_d, \tau, n_\Delta}^{(N, L)} \sqrt{N - n_d} &= [\Gamma_N^{(L)}(\beta)]^{-1/2} f_{\tau, n_\Delta}^{(L)} \frac{\beta^{n_d}}{[(N - n_d - 1)!(n_d - \tau)!(n_d + \tau + 3)!!]^{1/2}} \\ &= \left(\frac{\Gamma_N^{(L)}(\beta)}{\Gamma_{N-1}^{(L)}(\beta)} \right)^{-1/2} \xi_{n_d, \tau, n_\Delta}^{(N-1, L)} \end{aligned} \quad (\text{C.1.2})$$

so that:

$$\begin{aligned} s|\beta; N, L\rangle &= \sum_{\tau \leq n_d \leq N, \tau, n_\Delta} \frac{1}{2} [1 + (-1)^{n_d - \tau}] \xi_{n_d, \tau, n_\Delta}^{(N, L)} s|N, n_d, \tau, n_\Delta, L\rangle \\ &= \sum_{\tau \leq n_d \leq N-1, \tau, n_\Delta} \frac{1}{2} [1 + (-1)^{n_d - \tau}] \xi_{n_d, \tau, n_\Delta}^{(N, L)} \sqrt{N - n_d} |N - 1, n_d, \tau, n_\Delta, L\rangle \\ &= \left(\frac{\Gamma_N^{(L)}(\beta)}{\Gamma_{N-1}^{(L)}(\beta)} \right)^{-1/2} \sum_{\tau \leq n_d \leq N-1, \tau, n_\Delta} \frac{1}{2} [1 + (-1)^{n_d - \tau}] \xi_{n_d, \tau, n_\Delta}^{(N-1, L)} |N - 1, n_d, \tau, n_\Delta, L\rangle \\ &= \left(\frac{\Gamma_N^{(L)}(\beta)}{\Gamma_{N-1}^{(L)}(\beta)} \right)^{-1/2} |\beta; N - 1, L\rangle \end{aligned} \quad (\text{C.1.3})$$

or more generally:

$$s^n |\beta; N, L\rangle = \left(\frac{\Gamma_N^{(L)}(\beta)}{\Gamma_{N-n}^{(L)}(\beta)} \right)^{-1/2} |\beta; N - n, L\rangle \quad (\text{C.1.4})$$

Calculating $\langle \beta_1; N, L | \beta_2; N, L \rangle$

The dependence on β , beside the total normalization, is only in the β^{n_d} term. In addition we note that Γ depends only on its argument squared, so that $\Gamma(-\beta^{1/2}) = \Gamma(\beta^{1/2})$ (the value of Γ is given in Eq. (6.5), page 52). Using the

above, we have

$$\begin{aligned}
r_{12} &= \langle \beta_1; N, L | \beta_2; N, L \rangle = \\
&= [\Gamma_N^{(L)}(\beta_1) \Gamma_N^{(L)}(\beta_2)]^{-1/2} \sum_{\tau, n_d, n_\Delta} \frac{(\beta_1 \beta_2)^{n_d} (f_{\tau, n_\Delta}^{(L)})^2}{(N - n_d)! (n_d - \tau)! (n_d + \tau + 3)!} \\
&= [\Gamma_N^{(L)}(\beta_1) \Gamma_N^{(L)}(\beta_2)]^{-1/2} \frac{\Gamma_N^{(L)}(\sqrt{\beta_1 \beta_2})}{\Gamma_N^{(L)}(\sqrt{\beta_1 \beta_2})} \sum_{\tau, n_d, n_\Delta} \frac{[(\sqrt{\beta_1 \beta_2})^{n_d} f_{\tau, n_\Delta}^{(L)}]^2}{(N - n_d)! (n_d - \tau)! (n_d + \tau + 3)!} \\
&= \frac{[\Gamma_N^{(L)}(\beta_1) \Gamma_N^{(L)}(\beta_2)]^{-1/2}}{\Gamma_N^{(L)}(\sqrt{\beta_1 \beta_2})^{-1}} = \frac{\Gamma_N^{(L)}(\sqrt{\beta_1 \beta_2})}{[\Gamma_N^{(L)}(\beta_1) \Gamma_N^{(L)}(\beta_2)]^{1/2}}
\end{aligned} \tag{C.1.5}$$

Calculating $\langle \beta_1; N, L | (s^\dagger)^n (s^\dagger)^n \beta_2; N, L \rangle$

Using Eqs. (C.1.4)-(C.1.5) we have

$$\begin{aligned}
\langle \beta_1; N, L | (s^\dagger)^n s^n \beta_2; N, L \rangle &= \left(\frac{\Gamma_N^{(L)}(\beta_1)}{\Gamma_{N-n}^{(L)}(\beta_1)} \right)^{-1/2} \left(\frac{\Gamma_N^{(L)}(\beta_2)}{\Gamma_{N-n}^{(L)}(\beta_2)} \right)^{-1/2} \frac{[\Gamma_{N-n}^{(L)}(\beta_1) \Gamma_{N-n}^{(L)}(\beta_2)]^{-1/2}}{\Gamma_{N-n}^{(L)}(\sqrt{\beta_1 \beta_2})^{-1}} \\
\Rightarrow S_{n,L}^{(N)}(\beta_1, \beta_2) &\equiv \langle \beta_1; N, L | (s^\dagger)^n s^n | \beta_2; N, L \rangle = \frac{\Gamma_{N-n}^{(L)}(\sqrt{\beta_1 \beta_2})}{[\Gamma_N^{(L)}(\beta_1) \Gamma_N^{(L)}(\beta_2)]^{1/2}}
\end{aligned} \tag{C.1.6}$$

Note that $S_{0,L}^{(N)} = \langle \beta_1; N, L | \beta_2; N, L \rangle = r_{12}$

Calculating ‘‘sandwiching’’ of various operators between the intrinsic states

Below we use the following notations to make it more readable. All terms are L -dependent, but since the Hamiltonian is $O(3)$ scalar, different L 's do not mix:

$$\begin{aligned}
\Gamma_N(\beta) &\equiv \Gamma_N^{(L)}(\beta) \\
\Gamma_N(\beta_1, \beta_2) &\equiv \Gamma_N(\beta_1) \Gamma_N(\beta_2) \\
S_n^N(\beta_1, \beta_2) &\equiv S_{n,L}^{(N)}(\beta_1, \beta_2)
\end{aligned} \tag{C.1.7}$$

Calculating $\langle \beta_1; N, L | \hat{n}_d | \beta_2; N, L \rangle$

$$\langle \beta_1; N, L | \hat{n}_d | \beta_2; N, L \rangle \equiv D_{1,L}^{(N)}(\beta_1, \beta_2) = NS_0^N(\beta_1, \beta_2) - S_1^N(\beta_1, \beta_2) \quad (\text{C.1.8})$$

Calculating $\langle \beta_1; N, L | \hat{n}_d(\hat{n}_d - 1) | \beta_2; N, L \rangle$

We have:

$$\hat{n}_d(\hat{n}_d - 1) = (N - \hat{n}_s)(N - \hat{n}_s - 1) = N(N - 1) + 2(1 - N)\hat{n}_s + \hat{n}_s(\hat{n}_s - 1)$$

so that

$$\begin{aligned} \langle \beta_1; N, L | \hat{n}_d(\hat{n}_d - 1) | \beta_2; N, L \rangle &\equiv D_{2,L}^{(N)}(\beta_1, \beta_2) \\ &= N(N - 1)S_0^N(\beta_1, \beta_2) - 2(N - 1)S_1^N(\beta_1, \beta_2) + S_2^N(\beta_1, \beta_2) \end{aligned} \quad (\text{C.1.9})$$

Calculating $\langle \beta_1; N, L | \hat{C}_{O(3)} | \beta_2; N, L \rangle$

$$\langle \beta_1; N, L | \hat{C}_{O(3)} | \beta_2; N, L \rangle = S_0^N L(L + 1) \quad (\text{C.1.10})$$

Calculating $\langle \beta_1; N, L | \hat{n}_d^2 | \beta_2; N, L \rangle$

We note that:

$$\hat{n}_d^2 = (N - \hat{n}_s)^2 = N^2 - 2N\hat{n}_s + \hat{n}_s^2$$

and since $(s^\dagger)^2 s^2 = (\hat{n}_s - 1)\hat{n}_s$ we get:

$$\hat{n}_d^2 = N^2 - (2N + 1)\hat{n}_s + s^\dagger s^\dagger s s$$

so that

$$\langle \beta_1; N, L | \hat{n}_d^2 | \beta_2; N, L \rangle = N^2 S_0^N(\beta_1, \beta_2) - (2N + 1)S_1^N(\beta_1, \beta_2) + S_2^N(\beta_1, \beta_2) \quad (\text{C.1.11})$$

(or using the above results: $\hat{n}_d^2 = \hat{n}_d(\hat{n}_d - 1) + \hat{n}_d$ we have: $\langle \beta_1; N, L | \hat{n}_d^2 | \beta_2; N, L \rangle = D_{2,L}^{(N)}(\beta_1, \beta_2) + D_{1,L}^{(N)}(\beta_1, \beta_2)$)

Calculating $\langle \beta_1; N, L | \hat{C}_{O(5)} | \beta_2; N, L \rangle$

First we note that we can write [24]:

$$-\hat{C}_{O(5)} + \hat{n}_d(\hat{n}_d + 3) = (d^\dagger \cdot d^\dagger)(\tilde{d} \cdot \tilde{d})$$

\hat{n}_d, \hat{n}_d^2 are already known. We need to calculate $(d^\dagger \cdot d^\dagger)(\tilde{d} \cdot \tilde{d})$. This is done by noting that the condensate $|\beta, 0; N\rangle$ is annihilated by $P_0 = d \cdot d - \beta^2 s^2$. In addition because P_0 is $O(3)$ scalar, it does not mix different L irreps, so that $P_0|\beta; N, L\rangle = 0$. Using this we have

$$(\tilde{d} \cdot \tilde{d})|\beta_2; N, L\rangle = (P_0 + \beta_2^2 s^2)|\beta_2; N, L\rangle = \beta_2^2 s^2|\beta_2; N, L\rangle$$

so that

$$\langle \beta_1; N, L | (d^\dagger \cdot d^\dagger)(\tilde{d} \cdot \tilde{d}) | \beta_2; N, L \rangle = (\beta_1 \beta_2)^2 S_2^N(\beta_1, \beta_2)$$

and

$$\begin{aligned} \langle \beta_1; N, L | \hat{C}_{O(5)} | \beta_2; N, L \rangle = \\ 4D_1^N(\beta_1, \beta_2) + D_2^N(\beta_1, \beta_2) - (\beta_1 \beta_2)^2 S_2^N(\beta_1, \beta_2) \end{aligned} \quad (\text{C.1.12})$$

Calculating $\langle \beta_1; N, L | \hat{C}_{O(6)} | \beta_2; N, L \rangle$

We note that [24]:

$$-\hat{C}_{O(6)} + N(N + 4) = [(s^\dagger)^2 + d^\dagger \cdot d^\dagger][h.c.]$$

and using the same method as before:

$$\begin{aligned} (s^2 + \tilde{d} \cdot \tilde{d})|\beta_2; N, L\rangle &= (s^2 + P_0 + \beta_2^2 s^2)|\beta_2; N, L\rangle \\ &= (1 + \beta_2^2)s^2|\beta_2; N, L\rangle \end{aligned}$$

and we have:

$$\langle \beta_1; N, L | \hat{C}_{O(6)} | \beta_2; N, L \rangle = N(N+4)S_0^N(\beta_1, \beta_2) - (1 + \beta_1^2)(1 + \beta_2^2)S_2^N(\beta_1, \beta_2) \quad (\text{C.1.13})$$

Calculating $\langle \beta_1; N, L | \hat{n}_d \hat{C}_{O(5)} | \beta_2; N, L \rangle$

We have $\hat{n}_d \hat{C}_{O(5)} = (N - \hat{n}_s) \hat{C}_{O(5)}$. The first part is immediate, for the second we note that $[s, \hat{C}_{O(5)}] = 0$ so that:

$$\hat{n}_s \hat{C}_{O(5)} = s^\dagger s \hat{C}_{O(5)} = s^\dagger \hat{C}_{O(5)} s$$

and using Eq. (C.1.4) and Eq. (C.1.12) we get

$$\begin{aligned} \langle \beta_1; N, L | \hat{n}_s \hat{C}_{O(5)} | \beta_2; N, L \rangle &= \\ &\left(\frac{\Gamma_N(\beta_2)}{\Gamma_{N-1}(\beta_2)} \frac{\Gamma_N(\beta_1)}{\Gamma_{N-1}(\beta_1)} \right)^{-1/2} \times \\ &(4D_1^{N-1}(\beta_1, \beta_2) + D_2^{N-1}(\beta_1, \beta_2) - (\beta_1 \beta_2)^2 S_2^{N-1}(\beta_1, \beta_2)) \end{aligned} \quad (\text{C.1.14})$$

The above results can be now combined into m_{ij} of Eq. (6.4).

C.2 Calculating the Transition Probability Between L -Projected States

The reduced transition probability between the L -projected states of two states with given K : $|\alpha K\rangle$ and $|\alpha' K'\rangle$ [22] is:

$$B(E2; \alpha K L \rightarrow \alpha' K' L') = \frac{|\Sigma_{\mu}(LK 2\mu|L'K + \mu) \int d\tau d_{K'K+\mu}^{(L')*}(\theta) \langle \alpha', K' | R(\theta) T_{\mu}^{(2)} | \alpha K \rangle|^2}{\langle \alpha' K' | \int d\tau d_{K'K'}^{(L')*}(\theta) R(\theta) | \alpha' K' \rangle \langle \alpha K | \int d\tau d_{KK}^{(L)*}(\theta) R(\theta) | \alpha K \rangle}$$

Here $d\tau = d(\cos \theta)$ with the integration limits $\theta \in [0, \pi]$ and $T^{(2)} = d^{\dagger} s + s^{\dagger} \tilde{d} + \chi(d^{\dagger} \tilde{d})^{(2)}$ ($e_b = 1$). This expression will be calculated using $|\alpha K = 0\rangle \equiv |\beta_2\rangle = (s^{\dagger} + \beta_2 d_0^{\dagger})^N |0\rangle$ and $|\alpha' K' = 0\rangle \equiv |\beta_1\rangle = (s^{\dagger} + \beta_1 d_0^{\dagger})^N |0\rangle$. Beginning with the numerator, the first term to be calculated is $d_i^{\dagger} s + s^{\dagger} \tilde{d}_i$. Note that $s^{\dagger} \tilde{d}_i$ is zero unless $i = 0$. The other half of this expression is (Einstein summation applies and $d_{ij}^{(2)} \equiv d_{ij}^{(2)}(\theta)$):

$$\begin{aligned} \langle 0 | (\beta_1 d_0 + s)^N R(\theta) d_i^{\dagger} s (\beta_2 d_0^{\dagger} + s^{\dagger})^N | 0 \rangle &= \\ N \langle 0 | (\beta_1 d_0 + s)^N d_{ji}^{(2)} d_j^{\dagger} (\beta_2 d_{k0}^{(2)} d_k^{\dagger} + s^{\dagger})^{N-1} | 0 \rangle &= \quad (\text{applying } s \text{ to the right} \\ &\quad \text{and rotating)} \\ N^2 d_{ji}^{(2)} \beta_1 \delta_{j0} \langle 0 | (\beta_1 d_0 + s)^{N-1} (\beta_2 d_{k0}^{(2)} d_k^{\dagger} + s^{\dagger})^{N-1} | 0 \rangle &= \quad (\text{applying } d_j^{\dagger} \text{ to the left)} \\ N^2 d_{0i}^{(2)} \beta_1 \langle 0 | (\beta_1 d_0 + s)^{N-1} (\beta_2 d_{k0}^{(2)} d_k^{\dagger} + s^{\dagger})^{N-1} | 0 \rangle & \end{aligned} \quad (\text{C.2.1})$$

Using the relation:

$$\begin{aligned} [B, A^{\dagger}] = \lambda, \quad B|0\rangle = 0, \quad \langle 0|A^{\dagger} = 0, \quad \langle 0|0\rangle = 1 \\ \Rightarrow \langle 0|B^N (A^{\dagger})^N |0\rangle = N! \lambda^N \end{aligned} \quad (\text{C.2.2})$$

and

$$[\beta_1 d_0 + s, \beta_2 d^{(2)}(\theta)_{k0} d_k^{\dagger} + s^{\dagger}] = 1 + \beta_1 \beta_2 d^{(2)}(\theta)_{k0} \delta_{k0} = 1 + \beta_1 \beta_2 d_{00}^{(2)} \quad (\text{C.2.3})$$

we have

$$\begin{aligned} N^2 d_{0i}^{(2)}(\theta) \beta_1 \langle 0 | (\beta_1 d_0 + s)^{N-1} (\beta_2 d_{k0}^{(2)}(\theta) d_k^\dagger + s^\dagger)^{N-1} | 0 \rangle = \\ NN! d_{0i}^{(2)}(\theta) \beta_1 (1 + \beta_1 \beta_2 d_{00}^{(2)})^{N-1} \end{aligned} \quad (\text{C.2.4})$$

Similarly for $s^\dagger d_0$ we have

$$\begin{aligned} \langle 0 | (\beta_1 d_0 + s)^N R(\theta) s^\dagger d_0 (\beta_2 d_0^\dagger + s^\dagger)^N | 0 \rangle = & \quad (\text{applying } \leftarrow s^\dagger, d_0 \rightarrow) \\ N^2 \beta_2 \langle 0 | (\beta_1 d_0 + s)^{N-1} (\beta_2 d_{k0}^{(2)}(\theta) d_k^\dagger + s^\dagger)^{N-1} | 0 \rangle = \\ NN! \beta_2 (1 + \beta_1 \beta_2 d_{00}^{(2)})^{N-1} \end{aligned} \quad (\text{C.2.5})$$

For the full expression involving $d_i^\dagger s + s^\dagger d$ we have:

$$\begin{aligned} \int d\tau d_{0i}^{(L')*}(\theta) \langle K' | R(\theta) d_i^\dagger s + s^\dagger d_i | K \rangle = \\ NN! \int d\tau d_{0i}^{(L')*}(\theta) [\beta_1 d_{0i}^{(2)}(\theta) + \delta_{i0} \beta_2] (1 + \beta_1 \beta_2 d_{00}^{(2)})^{N-1} \end{aligned} \quad (\text{C.2.6})$$

The other term $(d^\dagger \tilde{d})_i^{(2)}$ can be calculated in a similar manner (remember that $(d^\dagger \tilde{d})_i^{(2)} = \sum_{M', M} (2M \ 2M' | 2i) (-1)^{M'} d_M^\dagger d_{-M'}$):

$$\begin{aligned} \langle 0 | (\beta_1 d_0 + s)^N R(\theta) (d^\dagger \tilde{d})_i^{(2)} (\beta_2 d_0^\dagger + s^\dagger)^N | 0 \rangle = \\ \sum_{M', M} (2M \ 2M' | 2i) (-1)^{M'} \langle 0 | (\beta_1 d_0 + s)^N R(\theta) d_M^\dagger d_{-M'} (\beta_2 d_0^\dagger + s^\dagger)^N | 0 \rangle = \\ (2i \ 20 | 2i) \langle 0 | (\beta_1 d_0 + s)^N R(\theta) d_i^\dagger d_0 (\beta_2 d_0^\dagger + s^\dagger)^N | 0 \rangle = \\ N \beta_2 (2i \ 20 | 2i) \langle 0 | (\beta_1 d_0 + s)^N R(\theta) d_i^\dagger (\beta_2 d_0^\dagger + s^\dagger)^N | 0 \rangle = \\ N^2 \beta_2 (2i \ 20 | 2i) d_{0i}^{(2)}(\theta) \beta_1 \langle 0 | (\beta_1 d_0 + s)^{N-1} (\beta_2 d_{k0}^{(2)}(\theta) d_k^\dagger + s^\dagger)^{N-1} | 0 \rangle \end{aligned} \quad (\text{C.2.7})$$

Using the above result, we have :

$$\begin{aligned} \int d\tau d_{0i}^{(L')*}(\theta) \langle \beta_1 | R(\theta) (d^\dagger \tilde{d})_i^{(2)} | \beta_2 \rangle = \\ N \beta_2 \beta_1 (2i \ 20 | 2i) NN! \int d\tau d_{0i}^{(L')*}(\theta) d_{0i}^{(2)}(\theta) (1 + \beta_1 \beta_2 d_{00}^{(2)})^{N-1} \end{aligned} \quad (\text{C.2.8})$$

The denominator is calculated as :

$$\begin{aligned}
& \int d\tau d_{00}^{(L)*} \langle 0 | (s + \beta d_0)^N R(\theta) (s^\dagger + \beta d_0^\dagger)^N | 0 \rangle = \\
& \int d\tau d_{00}^{(L)*} \langle 0 | (s + \beta d_0)^N (s^\dagger + \beta d_{i0}^{(2)}(\theta) d_i^\dagger)^N | 0 \rangle = \quad (C.2.9) \\
& N! \int d\tau d_{00}^{(L)*}(\theta) (1 + \beta^2 d_{00}^{(2)}(\theta))^N
\end{aligned}$$

Summing everything we have

$$\begin{aligned}
B(E2; \beta_2 L \rightarrow \beta_1 L') = \\
& \frac{N^2 |\Sigma_\mu(L0\ 2\mu|L'\mu) \int d\tau d_{0\mu}^{(L)*} [\beta_1 d_{0\mu}^{(2)} + \delta_{\mu 0} \beta_2 + \chi \beta_2 \beta_1 (2\mu\ 20|2\mu) d_{0\mu}^{(2)}] (1 + \beta_1 \beta_2 d_{00}^{(2)})^{N-1}|^2}{\left(\int d\tau d_{00}^{(L)*} (1 + \beta_1^2 d_{00}^{(2)})^N \right) \left(\int d\tau d_{00}^{(L)*} (1 + \beta_2^2 d_{00}^{(2)})^N \right)} \\
& d_{M'M}^{(L)} = \langle LM' | e^{-i\theta L_y} | LM \rangle \quad (C.2.10)
\end{aligned}$$

and the same calculation is used to calculate the reduced matrix terms:

$$\begin{aligned}
(2L+1)^{-1/2} \langle \beta_1 L' || T^{(\lambda)} || \beta_2 L \rangle = \\
& \frac{N \left(\Sigma_\mu(L0\ 2\mu|L'\mu) \int d\tau d_{0\mu}^{(L)*} [\beta_1 d_{0\mu}^{(2)} + \delta_{\mu 0} \beta_2 + \chi \beta_2 \beta_1 (2\mu\ 20|2\mu) d_{0\mu}^{(2)}] (1 + \beta_1 \beta_2 d_{00}^{(2)})^{N-1} \right)}{\left(\int d\tau d_{00}^{(L)*} (1 + \beta_1^2 d_{00}^{(2)})^N \right)^{1/2} \left(\int d\tau d_{00}^{(L)*} (1 + \beta_2^2 d_{00}^{(2)})^N \right)^{1/2}} \\
& d_{MM'}^{(L)} \equiv d_{MM'}^{(L)}(\theta) \quad (C.2.11)
\end{aligned}$$